NeuroImage 114 (2015) 71–87

Contents lists available at ScienceDirect

NeuroImage

journal homepage: www.elsevier.com/locate/ynimg

A cytoarchitecture-driven myelin model reveals area-specific signatures in human primary and secondary areas using ultra-high resolution in-vivo brain MRI

J. Dinse [a,b,c,*], N. Härtwich [a], M.D. Waehnert [a], C.L. Tardif [a,b], A. Schäfer [a], S. Geyer [a], B. Preim [c], R. Turner [a], P.-L. Bazin [a,b]

[a] Department of Neurophysics, Max Planck Institute for Human Cognitive and Brain Sciences, Stephanstraß e 1a, 04103 Leipzig, Germany
[b] Department of Neurology, Max Planck Institute for Human Cognitive and Brain Sciences, Stephanstraß e 1a, 04103 Leipzig, Germany
[c] Faculty of Computer Science, Otto von Guericke University, Universitätsplatz 2, 39106 Magdeburg, Germany

ARTICLE INFO

Article history:
Received 9 July 2014
Accepted 9 April 2015
Available online 18 April 2015

Keywords:
Cytoarchitecture
Myeloarchitecture
Cortical areas
Cortical profiles
Modelling ultra-high resolution
Quantitative MRI

ABSTRACT

This work presents a novel approach for modelling laminar myelin patterns in the human cortex in brain MR images on the basis of known cytoarchitecture. For the first time, it is possible to estimate intracortical contrast visible in quantitative ultra-high resolution MR images in specific primary and secondary cytoarchitectonic areas. The presented technique reveals different area-specific signatures which may help to study the spatial distribution of cortical T_1 values and the distribution of cortical myelin in general. It may lead to a new discussion on the concordance of cyto- and myeloarchitectonic boundaries, given the absence of such concordance atlases. The modelled myelin patterns are quantitatively compared with data from human ultra-high resolution in-vivo 7 T brain MR images (9 subjects). In the validation, the results are compared to one post-mortem brain sample and its ex-vivo MRI and histological data. Details of the analysis pipeline are provided. In the context of the increasing interest in advanced methods in brain segmentation and cortical architectural studies, the presented model helps to bridge the gap between the microanatomy revealed by classical histology and the macroanatomy visible in MRI.

Introduction

The human brain is a highly convoluted organ with many folds and fissures. Neural activity and functional processing occur in deep grey matter and in the 2–5 mm thick cortex. The cortex has the topology of a 2-dimensional sheet and consists, in the isocortex, of six cytoarchitectonic layers. Cortical layer structure has been investigated for more than a century (Baillarger, 1840; Brodmann, 1909). During the 20th century, cortical cartographers distinguished cortical areas mainly based on cytoarchitectonic criteria, i.e. the size, shape, and density of the cells as well as their arrangement and organisation.

In order to provide precise mapping of structure and function onto the brain surface, two major neuroanatomical disciplines evolved: histological studies of cytoarchitecture and myeloarchitecture. Brodmann (1909) pioneered cytoarchitectural studies of the cortex. He focussed on the spatial distributions of cell bodies and produced the first qualitative descriptions and quantitative layer-specific measures in different cortical areas. Later, von Economo and Koskinas (1925) published a full set of tables for 52 cortical and subcortical areas, including absolute and relative values for different measures per layer. These include layer thickness, cell density, and cell size. More recently, a 3-dimensional (3D) digital probabilistic cytoarchitectural atlas based on stained and registered histological sections of ten post-mortem brains was introduced by Eickhoff et al. (2005a). Neuroscientists commonly regard such cytoarchitectonically-derived probabilistic Brodmann area maps as useful guides to cortical localisation.

Related work using classical histology

In contrast with cytoarchitecture, myeloarchitecture has been largely neglected during the past hundred years. This discipline examines the arrangement of tangentially and radially oriented myelinated fibres in preparations stained for myelin sheaths. Research in this field is incomplete, inconclusive, or even contradictory. Quantitative methods were not available to the pioneers in this field, Cécile and Oskar Vogt (Vogt and Vogt, 1919a,b; Vogt, 1923). The Vogts characterised most of their findings using highly subjective terms as “thin to thick”, “poorly to highly dense” or “less to fully present”, which do not lend themselves

* Corresponding author at: Department of Neurophysics, Max Planck Institute for Human Cognitive and Brain Sciences, Stephanstraß e 1a, 04103 Leipzig, Germany.
E-mail address: dinse@cbs.mpg.de (J. Dinse).

http://dx.doi.org/10.1016/j.neuroimage.2015.04.023

to reproducible assessments. Little has been done since then to develop more objective measures and criteria. Adolf Hopf and Valentin Braitenberg were the first to report quantitative cortical profiles associated with myelin. A cortical profile describes a traverse running from the inner to the outer cortical boundary along which intensity values can be sampled (Hopf, 1968, 1969, 1970; Braitenberg, 1962). Their work is based on the photometric reproduction of sections stained for myelin. However, Braitenberg studied the fibre density in cortical areas, whereas Hopf focused on the myelinisation in the cortex which describes the development of the myelin sheath around a nerve fibre. Fibre density and myelin are certainly interlinked, but Hopf was convinced that the content or concentration of myelin in the cortex does not only depend on the fibre density, but also on the fibre calibre. Only recently, Nieuwenhuys et al. (2014) published a unique myeloarchitectonic mapping incorporating information from the Vogt–Vogt School. The mapping is a non-digital 2D projection onto a standard reference brain. To date, a widely accepted comprehensive myeloarchitectural reference atlas comparable to the digital probabilistic cytoarchitectural atlas presented by Eickhoff et al. (2005a) does not exist. Even today, little is known about the concordance between cortical cytoarchitectonic and myeloarchitectonic boundaries. Hence, the question arises whether the construction of a myeloarchitectonic atlas is now feasible, and whether this can be achieved by a quantitative generalisation of the Vogts' concepts.

The Vogts focussed on classifying patterns of fibres radial to the underlying white matter, and on subtle cortical layer-dependent details, which led to a confusing proliferation of categories and subcategories. By contrast, Hopf followed Elliot Smith (1907) in noting that different patterns of myeloarchitecture were well discriminated by variations in the myelination of deeper cortical layers. Hopf especially focussed on the so-called bands of Baillarger (Baillarger, 1840), two heavily myelinated transverse layers, the outer band usually coinciding with cytoarchitectonic layer IV (*Lamina granularis interna*), and the inner band with cytoarchitectonic layer V (*Lamina pyramidalis interna*) (Hopf, 1967; Vogt, 1910) (see Fig. 1A). In analysing the appearance of the bands of Baillarger, Hopf utilised the Vogts' most practical criterion: comparing local features of the Baillarger stripes of one cortical area globally to other areas. In the mid-20th century, Hopf first used these criteria to systematically parcellate the cortical surface and generate a myeloarchitectonic map (Hopf, 1955, 1956; Hopf and Vitzthum, 1957).

Vogt (1910) categorised myeloarchitectonic areas into four main types: bistriate, unistriate, unitostriate, and astriate, depending on whether two horizontal myelin-rich bands are visible, only one band, or no striation at all. In Fig. 1B, we depict a semidiagrammatic representation of the myeloarchitectonic types of the cortex (reproduced from Hopf (1968, 1969)). The unistriate and unitostriate types both describe one band being visible. The unistriate type (Latin: unus) covers only one band while the unitostriate type (Latin from "unite") describes the fusion of multiple layers to a single visible one. The bistriate type has two visible bands. In contrast, the astriate type is so heavily myelinated that no individual bands are discernible. Hopf continued studying the bands of Baillarger and their position in cortical depth, their thickness, and their intensity of myelination. He found that differences between locally neighbouring areas may be much larger than those of areas far apart. This leads to a local categorisation into three minor types: an inner, an outer, and an equally dense myelinated type, depending on whether one of the bands, inner or outer, is more highly myelinated or whether both are equally myelinated. Extremes of these types can be found in well-studied primary cortical areas. The line of Gennari or Vicq d'Azyr (Gennari, 1782; Vicq d'Azyr, 1786) in the primary visual cortex (Brodmann area 17) is of unistriate type with an outer band of Baillarger being more pronounced.

It is apparent from classical histology that cytoarchitecture and myeloarchitecture are two aspects of the same anatomical reality, both reflecting cortical microarchitecture (Nieuwenhuys, 2013). Thus, it is reasonable to assume that there is a relationship between these

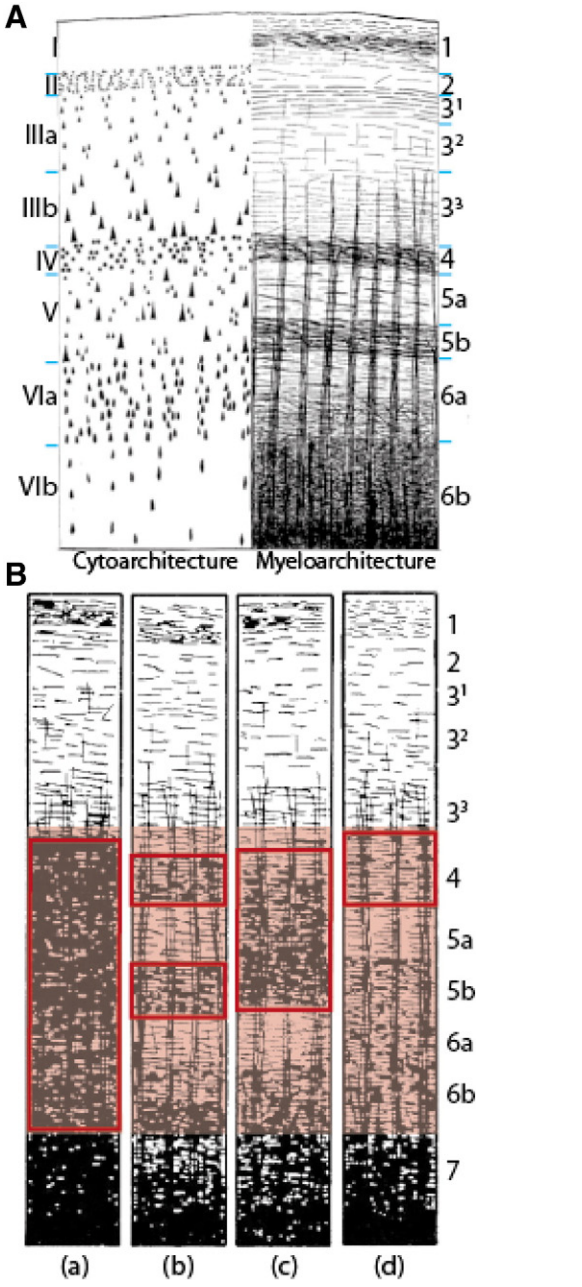

Fig. 1. A) The relationship in cortical microarchitecture between cytoarchitecture and myeloarchitecture. On the right side, the two (darker) bands of Baillarger (Baillarger, 1840), i.e. two heavily myelinated transverse layers, are visible. The outer band usually coincides with cytoarchitectonic layer IV (*Lamina granularis interna*) and the inner band with cytoarchitectonic layer V (*Lamina pyramidalis interna*) (Vogt, 1910). B) The four different types of myeloarchitecture remodelled from (Hopf, 1967; Vogt, 1910): a) astriate, b) bistriate, c) unitostriate, and d) unistriate. Lower cortical layers are highlighted in light red. The dashed boxes depict the bands of Baillarger.

two microstructural domains. Hellwig (1993) demonstrated in 14 cortical areas that a priori information derived from cytoarchitecture can be used to estimate relative cortical myelin density.

Recent developments in mapping myeloarchitecture using MRI

Since the pioneering study by Clark et al. (1992), researchers using MRI have found that image contrast in the cortex is mainly based on myelin (Walters et al., 2003, 2007; Eickhoff et al., 2005b). Intracortical contrast has been shown in group-average T_1 maps, T_2^* maps, and in

ratios between T_1-weighted and T_2-weighted images (Tardif et al., 2013; Geyer et al., 2011; Cohen-Adad et al., 2012; Deistung et al., 2013; Glasser and Van Essen, 2011; Sereno et al., 2012). Most of these contrasts is driven by myelin content, especially in quantitative T_1 maps. Geyer et al. (2011) demonstrated that 7 T MRI can reveal local cortical differences in quantitative T_1 images and, thus, can precisely depict some cortical boundaries. By using intracortical contrast in surface registration techniques, Tardif et al. (2013) demonstrated in a group-average T_1 map at a unique high resolution and for multiple cortical depths that T_1 maps actually reflect the cortical myeloarchitecture. Cortical profiles, e.g. traverses running perpendicularly through the depth of the cortex and sampling the image intensities, have allowed parcellations of primary areas in humans (Bridge and Clare, 2006; Dick et al., 2012; Dinse et al., 2013a; Annese et al., 2004; Schleicher et al., 2005) and primates (Bock et al., 2009).

Using cytoarchitectonic parcellations based on an observer-independent method (Eickhoff et al., 2005a) and surface registration, Fischl et al. (2008) were able to successfully provide probabilistic maps of cortical areas. Such maps are consistent with myeloarchitecture only in primary areas. Recently, generative models have become more popular for cortical parcellation and have been applied to functional or connectivity-based MRI data 9Lashkari et al., 2010; Sabuncu et al., 2009; Ryali et al., 2012).

New MRI mapping techniques allow one to image the brain at sub-millimetre resolution. With myelin being able to capture inter-areal differences, new approaches evolved that combine tonotopic fMRI and myeloarchitectonic T_1 mapping to localise primary visual areas (Sereno et al., 2012) and primary auditory areas (Lutti et al., 2014; Dick et al., 2012) in individual healthy adults.

Here, we present a generative approach which, based on known cytoarchitectural features, allows us to estimate cortical myelin patterns. The estimations are made in terms of in-vivo T_1 values (in milliseconds) as these have been shown to be associated with myelin content. The models thus represent the pattern of the in-vivo quantitative T_1 map that MRI should yield for a given area-specific cytoarchitecture. The modelled cortical patterns reveal different area-specific signatures and may be used for cortical parcellation based on purely intracortical features rather than probabilistic maps or cortical folding patterns. The method may also help to analyse the spatial distribution of cortical T_1 values. When cortical profiles are accurately defined (Waehnert et al., 2013b), intracortical features can be reliably observed in ultra-high resolution structural MRI data.

The model presented in this work was introduced in a recent conference paper by Dinse et al. (2013b). Here, we describe an improved implementation of the approach in detail. The capabilities of our cytoarchitectonically-driven myelin-based approach are demonstrated in the left primary motor (M1)/somatosensory (S1) region encompassing Brodmann areas 4, 3, 1, and 2. The model was applied and quantitatively compared to in-vivo images of nine subjects in order to show how much the signatures differ between areas. Validation was based on ex-vivo MR images and histological sections of one formalin-fixed post-mortem human brain. Additional validation experiments were conducted to study two important aspects of our approach:

1. How well can the area-specific models be distinguished when resolution increases or decreases?
2. How significant are the mean and the shape of a cortical profile compared to our approach?

Taken as a whole, this leads to the question whether the model can be used as a valid tool for myelin-based parcellation of the cortex. The method presented in this paper can be applied to other cortical areas. The approach may also provide new perspectives, both in imaging and in modelling the relationship between cytoarchitecture and myeloarchitecture, thus bringing about a better understanding of the functional and the structural organisation of the cortex in living humans.

Material and methods

The work presented here adapts Hellwig (1993)'s method and provides the first known application to in-vivo brain MR data. Therefore, in-vivo quantitative T_1 maps at ultra-high resolution of nine subjects were obtained with a 7 T (Tesla) MR scanner. Also, one post-mortem brain sample was used to obtain similar MR data as well as histological material.

Prerequisites: cortical profiles and layer estimation

At the core of the presented modelling approach are cortical profiles, i.e. traverses running from one cortical boundary surface to the other and along which image values can be sampled at different cortical depths. These profiles carry a rich information content (Bridge et al., 2005; Dinse et al., 2013a; Walters et al., 2007). With the in-vivo ultra-high resolution now used at 7 T, finer details of myelination, especially area-specific profile shapes, are revealed. To construct anatomically meaningful cortical profiles, we computationally divided the cortical sheet into multiple surfaces using a novel volume-preserving layering approach by Waehnert et al. (2013b). The estimated lamination parallels the cortical layers observed in myeloarchitecture (Bok, 1929). In locations of gyral crowns the outer layers are compressed while the inner layers are stretched out. In locations of sulcal fundi the opposite occurs. The layering model is based on volumetric segments that form a truncated cone and span the cortex from one boundary surface to the other representing the local cortical thickness. The areas of the top and bottom surfaces of a segment are proportional to the local curvature at the white matter (WM)/grey matter (GM) and GM/cerebrospinal fluid (CSF) boundary surfaces. The layering model transforms a desired volume fraction of the segment's volume into a distance fraction of the segment's cortical thickness. This transformation implicitly yields cortical depth estimates for each computed surface.

This section outlines the image acquisition and preprocessing of in-vivo data (Section 2.2.1) and post-mortem data (Section 2.2.2), i.e. ex-vivo MRI and histological data. The implemented methods are explained in detail by implementing and adapting the work of Hellwig (1993) (Section 2.3.1) followed by a description on how to transform the biological metrics into MRI metrics (Section 2.3.2). Finally, we defined a probabilistic metric to compute the similarity between area-specific models and single in-vivo cortical profiles within the entire cortex.

Data acquisition and preprocessing

In the following section, we will use the term layer to refer to anatomical layers originating from cyto- and myeloarchitectural studies. The term surfaces is reserved for computed layers i) representing the boundary surfaces between WM/GM and GM/CSF and ii) modelling the anatomical layering within the cortex.

In-vivo MRI

We scanned nine healthy human subjects (25.6 ± 3.0 years, five female subjects) with a MP2RAGE sequence (Marques et al., 2010) and a TR-FOCI pulse for inversion (Hurley et al., 2010) on a 7 Tesla (7 T) whole-body MR scanner (MAGNETOM 7 T, Siemens, Germany) using a 24 channel phased array coil (Nova Medical Inc., Wilmington, MA, USA). We obtained in-vivo whole-brain quantitative T_1 maps at 0.7 mm isotropic resolution (TI_1 / TI_2 = 900 = 2750 ms, TR = 5 s, TE = 2:45 ms, $\alpha 1$ / $\alpha 2$ = 5° / 3°, GRAPPA = 2, scan time = 11 min) and T_1 maps of each hemisphere separately at 0.5 mm isotropic resolution (same parameters, no GRAPPA, scan time = 30 min). The three maps were co-registered into a standard anatomical (Montreal Neurological Institute, MNI) reference space at 0.4 mm isotropic resolution and fused to generate a 0.4 mm whole-brain map from the two hemispheric 0.5 mm maps. In order to preserve cortical geometry, a rigid

registration was used optimized using a cost function of normalised mutual information. Fig. 2A depicts in anterior–posterior orientation an inflated in-vivo quantitative T_1 map (registered to 0.4 mm isotropic MNI space, 55% cortical depth) of a single subjects left hemisphere. Low T_1 values (ms) (blue) are associated with higher myelination. The white curve drawn on the inflated surface indicates the location of the MRI slice pictured to the right.

Cortical extraction was performed using the CRUISE algorithm Han et al., 2004 as integrated in the CBS Tools (Bazin et al., 2013). The surfaces between GM and WM and between GM and CSF were represented

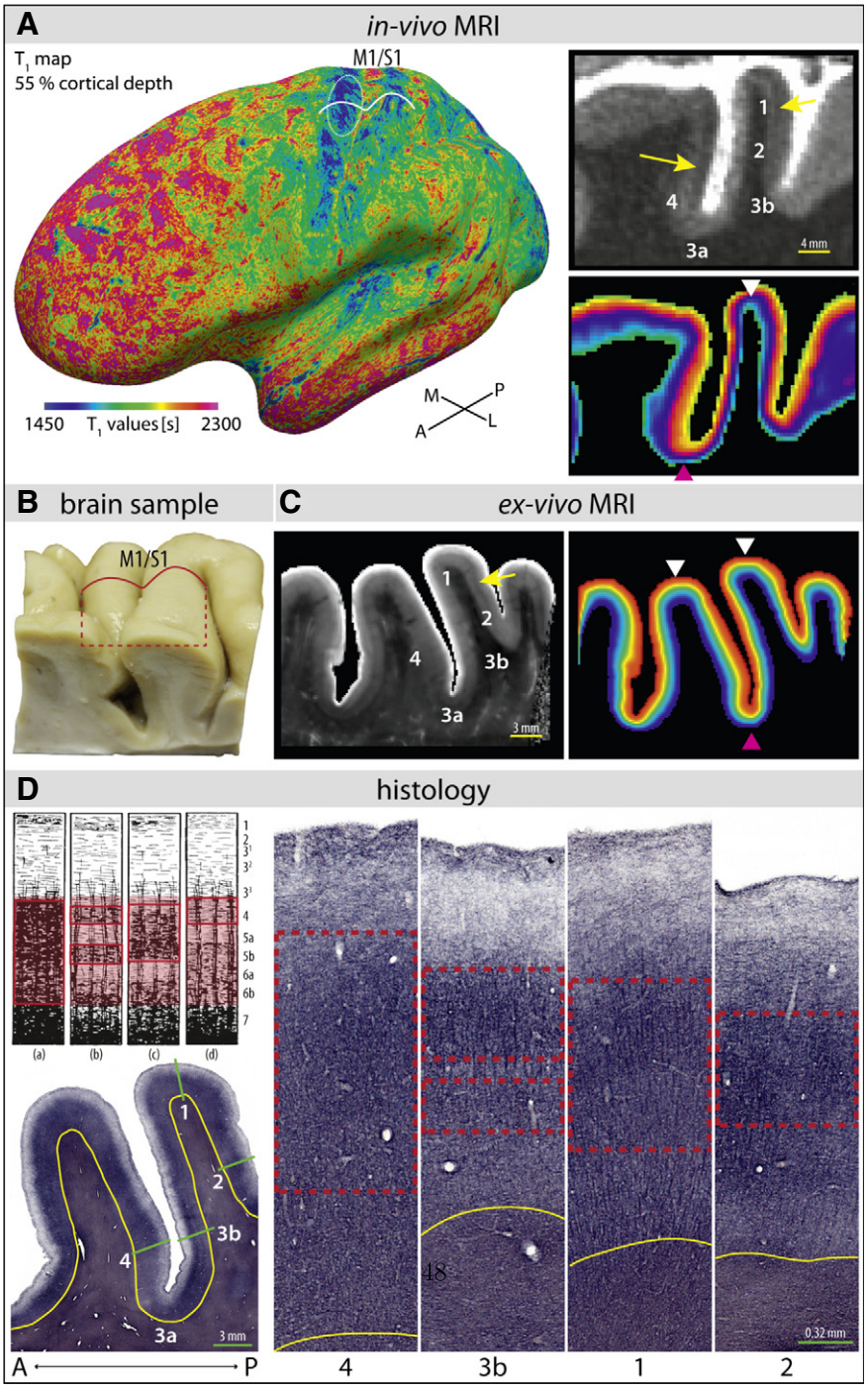

Fig. 2. Overview of material used in this work. A) Inflated 0.5 mm T_1 at 55% cortical depth. The M1/S1 region, known to be more highly myelinated, shows lower T_1 values. Variability in T_1 values is visible across the surface but also within M1 (encircled) which is related to the location of the motor hand knob. The white doublebow curve outlines the ROIs shown in the in-vivo T_1 map MRI slice ((A), upper right). BA 4 shows lower T_1 values than BA 3b. Striation (arrows) is visible. The image below depicts cortical depth values calculated using a novel volume-preserving layering approach (Waehnert et al., 2013b). In locations of gyral crowns (white arrowhead), the outer surfaces are compressed while the inner surfaces are stretched out. In locations of sulcal fundi (pink arrowhead), the behaviour of the surfaces changes to the opposite. B) The picture shows the brain sample used to derive ex-vivo data. The red doublebow curve covers our ROIs. C) Left: The image depicts the ex-vivo T_1 map MRI slice indicated as red curve in (B). BA 4 shows lower T_1 values than BA 3b. Striation is visible in BA 1 and 2 (arrow). Right: The layering depicts the cortical depth values. The behaviour of the laminae is the same as in (A) but much more visible due to the higher resolution of the ex-vivo MRI. D) The images illustrate the myelin stain and enlargements of it in locations of the green lines. The yellow line follows the WM boundary. Red boxes depict the Baillarger banding. As direct comparison, Hopf's illustrations Hopf (1967) presented in Fig. 1B are included.

in Cartesian space using a level-set framework (Sethian, 1999). The surfaces were used to estimate a set of $N = 20$ level-set surfaces based on the abovementioned volume-preserving approach. Fig. 2A, lower right, depicts the cortical depth estimates. Using the layered level-set surface representations, traverses were constructed that run from one cortical boundary surface to the other. Along these traverses, T_1 values of the MR image data were sampled to derive myelin-related profiles. For consistency, we will refer to these empirically-derived profiles as in-vivo profiles.

Ex-vivo MRI and histology

The ex-vivo data were used for verification only and were not used in the modelling of the area-specific MR patterns.

An ex-vivo brain sample of the left primary motor and somatosensory region, i.e. M1/S1 region, was analysed. Fig. 2B shows the brain sample used. The red curve outlines the region of interest. A formalin-fixed block of human post-mortem brain (age: 92 years, post-mortem time: 22 h) containing the pre- and post-central gyri was obtained from an autopsy with informed consent from the patient's relatives. No neurological or psychiatric pathologies were recorded for this brain.

The block was scanned in Fomblin (Solvay Solexis, Bollate, Italy) with a home-built dual-loop circularly polarised radio frequency (RF) coil. The MP2RAGE sequence was used to obtain a quantitative T_1 map of the M1/S1 region (0.25 mm isotropic resolution, TE = 2:94 ms, TR = 3000 ms, TI_1 = 325 ms, TI_2 = 900 ms, $\alpha1$ / $\alpha2$ = 8°/8°, 66 averages, actual scan time = 11 h 43 min).

In Fig. 2C we show the MRI slice at the red curve outlined in Fig. 2B. Estimation of the WM/GM and GM/CSF surfaces in the ex-vivo MR image was based on a manual segmentation of the data into WM and GM compartments. The surfaces were used to estimate a set of $N = 20$ level-set surfaces based on the above mentioned volume-preserving approach. The right picture in Fig. 2C illustrates the cortical depth estimates. Traverses were constructed and along these the post-mortem MR image T_1 values were sampled to generate myelin-related profiles. For consistency, we will refer to these post-mortem-derived profiles as ex-vivo profiles.

The same brain sample, containing Brodmann areas 4, 3, 1, and 2, was used for histological analysis. The block was cut with a freezing microtome (SM 2000R, LEICA Biosystems, Wetzlar, Germany). Consecutive sections were stained for myelin and cells and examined under an Axio Imager M1 light microscope (Zeiss, Jena, Germany) with a 5× objective at 2.58 μm in-plane resolution. In this work, only the myelin stains were considered. The cell stains were used for a general comparison of the underlying tissue structure. The sections (thickness: 30 μm) were immunostained for myelin sheaths (rabbit monoclonal antibody against myelin oligodendrocyte glycoprotein (MOG) diluted to 1:2000, avidin-biotin-peroxidase complex (ABC) method, chromogen: 3.3′-diaminobenzidine (DAB) tetrahydrochloride and ammonium nickel(II) sulfate). The floating sections were pre-treated in sodium borohydride (NaBH4) for 30 min at room temperature in order to enhance the antigen accessibility (Jäger et al., 2013).

Every other section of the same block was immunostained for cell bodies (mouse monoclonal antibody against neuronal marker protein HuC/HuD diluted to 1:400, ABC method, chromogen: DAB tetrahydrochloride and ammonium nickel(II) sulfate). The floating sections were pre-treated in Tris buffer (pH 8.0) for 20 min at 90 °C.

Consecutive sections alternate between cell and myelin stain. A complete 3D reconstruction of myelinated fibres in the cortex was therefore impossible. However, given 3D data, the volume-preserving method is able to provide cortical depth estimates. Therefore, one histological section was stacked six times to recover a 180 μm thick 3D data block. The section used is shown in Fig. 2D, lower left. The yellow line indicates the WM boundary. The zoomed-in pictures were taken from locations highlighted in green on the original stained section. As comparison, Vogt (1910) originally drawn illustrations remodelled by Hopf (1967) were included. The stacked data were manually segmented into WM and GM compartments and the volume-preserving approach was applied to estimate the intracortical surfaces. Due to the 2D nature of the histological sections and the implicitly given cortical depth estimates, the intensity values were averaged at different cortical depths to provide a myelin profile. For consistency, we will refer to such histologically-derived profiles as histology profiles.

Methods

In order to estimate laminar myelin density patterns as observed in quantitative T_1 maps, we established a model of cortical myeloarchitecture from known cytoarchitecture in a two-step approach. In the first step, we implemented and adapted Hellwig (1993)'s method. Quantitative properties of cytoarchitecture relevant in each cortical area found by von Economo and Koskinas (1925) were transformed into patterns representing myelin density. In a second step, we normalised the profiles into MRI space (T_1 values given in milliseconds) respecting the currently used MR resolution and MR imaging limitations such as partial voluming. Fig. 3 depicts the conceptual design of the presented approach including intermediate results. Finally, we build a probabilistic function based on a Gaussian metric that measures the similarity between area-specific models and in-vivo profiles obtained with ultra-high resolution brain MRI.

Generating cortical area-specific profiles

Hellwig's approach is based on two main assumptions:

1. Large neurons contribute more to intracortical myelin content than small ones.
2. The average distribution of horizontal axon collaterals of neurons can be quantified according to data provided by Paldino and Harth (1977).

Detailed information and a discussion of the assumptions can be found in Section 4.1.

We followed Hellwig's approach by first obtaining the relative thickness, mean neuronal cell density $c_{density}$, and mean cell size c_{size} for each cortical layer from the tabulations of von Economo and Koskinas (1925). The measures were given for locations in sulcal walls and gyral crowns. In case a Brodmann area was mainly located in a sulcal wall, we used the measures given for this location and, conversely, the measures for a gyral crown for areas mainly located on the crest of the gyrus. In von Economo and Koskinas (1925), the neuronal cell size c_{size} is defined as the ratio of $cell_{height}/cell_{width}$ of the cell body, which includes the nucleus. Note that the Nissl stain used by von Economo and Koskinas (1925) labels only cell bodies, not neurites. According to Hellwig (1993), myeloarchitecture can be estimated from cytoarchitecture by assuming that the quantity of myelin depends on the cell size, following a sigmoidal function s which describes the contribution of cells to the layer-specific myelin concentration. We modelled this relation as:

$$s(c_{size}) = \frac{1}{1 + exp(-r(c_{size} - l))} \quad (1)$$

in which l describes the location of maximum cellular contribution and r the rate of change (Fig. 3b).

An estimate of the initial cell content (Fig. 3c) for each layer c_{layer} was obtained as:

$$c_{layer} = c_{size}\ \ c_{density}\ \ s(c_{size}). \quad (2)$$

The laminar pattern of myelinated fibres in the cortex is considered to originate mainly from axonal collaterals of neuronal cells. To include laminar projections in the area-specific profile shapes and to transform the profile from cytoarchitectonic properties into information representing the myelin content, the initial cell content of c_{layer} was convolved with a function a describing the number of axonal collaterals

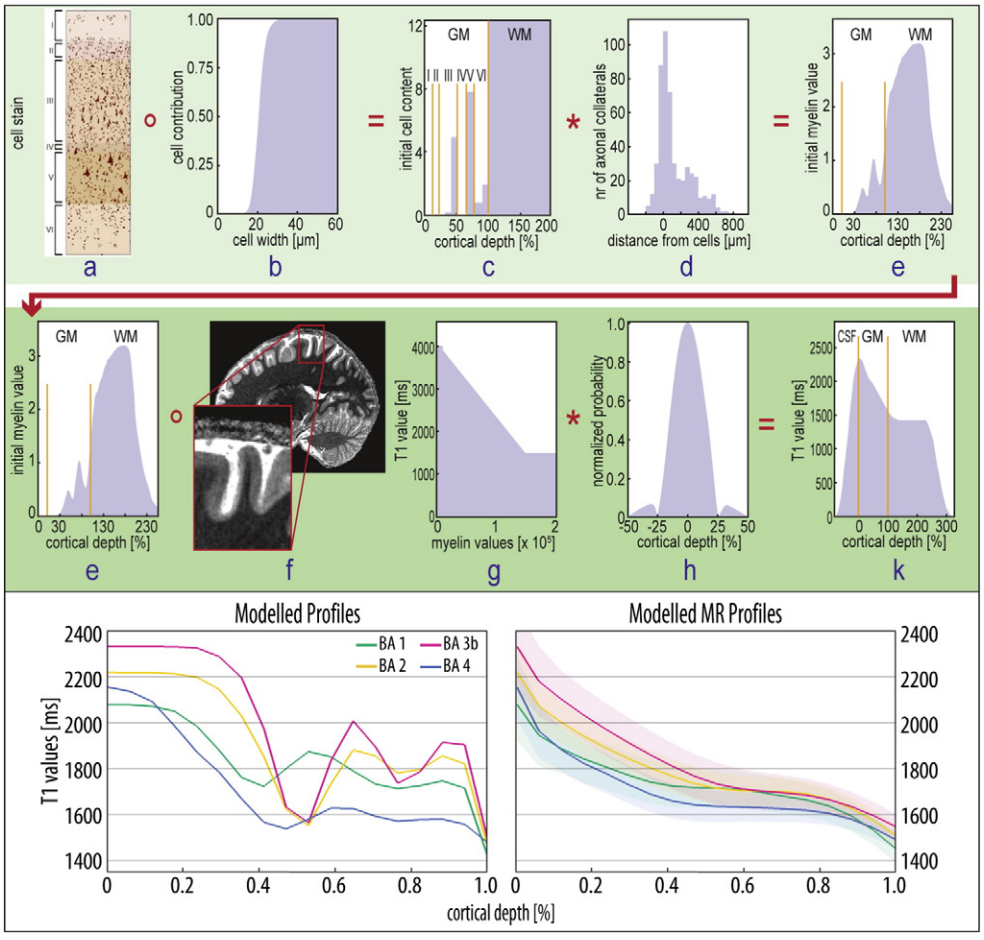

Fig. 3. Schematic overview of the processing pipeline. The top row illustrates the work by Hellwig (1993). Quantitative measures of cellular configuration are used to establish an initial cell content which is convolved with a model of the distribution of axonal collaterals. The second row transforms the modelled myelin-related profiles into modelled MR profiles of the T_1 intracortical contrast observable in brain MRI. In addition, the modelled (Fig. 3g) and modelled MR profiles (Fig. 3k) for each ROI are shown below.

distributed around a cell body remodelled from Paldino and Harth (1977) (see Fig. 3d):

$$m_{BA}(x) = \left(c_{layer} * a\right)(x)\mathrm{d}x. \tag{3}$$

The convolution is defined in the range of relative cortical depth $d \in [0, 1]$. The profiles m_{BA} give a qualitative indicator of myelin concentration in the cortex (Fig. 3e) (see Section 4.1 for discussion) and are comparable to myelin-stained sections and the myeloarchitecture described by Vogt and Vogt (1919a,b). In Section 4.1 we discuss in detail why the profiles are only qualitative.

Normalising area-specific profiles into the MR Imaging space

To allow for an application to quantitative MRI data, the area-specific models had to undergo two transformation steps.

Step 1 In step one we normalised the area-specific profiles into the MR intensity range of a quantitative T_1 map (values in milliseconds). This transformation step facilitates one to apply the model to individual subjects as well as to group data. This first transformation step has to respect further variability, i.e. partial volume effects in the cortex, originating from the rather coarse resolution of in-vivo MRI. The resulting profile is in MR intensity range, but still at the resolution of cell size given in the tabulations by von Economo and Koskinas (1925) (0.001 mm = 1 µm). The MR intensity range of the cortex is defined by the mean T_1 value and standard deviation of the boundary surfaces. We calculated these parameters directly from the WM/GM and the GM/CSF boundary surfaces, individually for each subject. However, the intensity range of T_1 values in individual areas varies and is, thus, defined as $I_{BA} = [I_{BA}^{wm}, I_{BA}^{csf}]$ for each individual Brodmann area. Please see Section 4.1 for a detailed discussion of causes of variability. The area-specific range was calculated by using the cortex' mean T_1 value μ and the cortex' T_1 standard deviation σ computed at the WM/GM boundary and the GM/CSF boundary (Fig. 3f) as follows:

$$I_{BA}^{wm} = \mu_{wm} - \hat{e}_{wm,BA}\sigma_{wm,BA} \tag{4}$$

and

$$I_{BA}^{csf} = \mu_{csf} - \hat{e}_{csf,BA}\sigma_{csf,BA}. \tag{5}$$

$\hat{e}_{wm}$ and $\hat{e}_{csf}$ represent the estimators of the determined area-specific variation at the two boundaries. $\hat{e}$ was estimated from prior investigations on lower resolution T_1 maps (0.7 mm

Table 1
Estimates $\hat{e}$, used in the normalisation step (Eqs. (4) and (5)), and estimated T_1 standard deviations σ^{modMR}, used in the profile similarity computation (Eq. (12)), are shown.

	$\hat{e}$				σ^{modMR}			
Estimates	BA 4	BA 3b	BA 1	BA 2	BA 4	BA 3b	BA 1	BA 2
WM	0.45	0.01	0.75	0.3	40	55	60	45
CSF	0.60	−0.1	0.90	0.35	140	185	160	135

isotropic) (Dinse et al., 2013a) in which the behaviour of the profiles in terms of mean and standard deviation has already been observed. Table 1 outlines the estimates.
Finally, the profiles in m_{BA} (Eq. (3)) were normalised into the T_1 MR intensity range of grey matter:

$$T_{1_{BA}}^{mod}(x) = I_{BA}^{wm} + \frac{\left(I_{BA}^{csf} - I_{BA}^{wm}\right)(m_{BA}(x) - min(m_{BA}(d)))}{max(m_{BA}(d)) - min(m_{BA}(d))} \quad (6)$$

in which $min()$ and $max()$ define the minimum and maximum of m_{BA} along relative cortical depth $d \in [0, 1]$ (Fig. 3g). At this point, the modelled T_1 profiles are continuous, but resemble the cell size resolution (0.001 mm) used in the atlas of von Economo and Koskinas (1925). For consistency, we refer to the modelled profiles $T_{1_{BA}}^{mod}$ in MR intensity range as modelled profiles.

Step 2 In the second step we transformed the modelled profiles into the currently used MR resolution. We build a filter function that can be understood as a translator between the model and different scales of MR resolution.
To match the limited MR resolution, the profiles in $T_{1_{BA}}^{mod}$ (Eq. (6)) were convolved with a windowed cardinal sine function that represents the MRI signal point-spread function (Fig. 3h). To take into account partial volume effects, the modelled profiles $T_{1_{BA}}^{mod}$ were extended into white and grey matter. T_1 values representing WM and CSF in MR images were taken from Rooney et al. (2007) and were assigned to the profile's end points corresponding to WM and CSF. The filter function intends to represent the current in-vivo MR image resolution. To account for the limiting effects of the MR resolution, we considered the relative overlap (in percent) between filter function and cortical thickness t_{BA} (in absolute value) in each Brodmann area (BA). We defined the width of the filter function as:

$$width = \frac{\mathrm{resMR}^{in-vivo}}{t_{BA}} t_m. \quad (7)$$

$\mathrm{resMR}^{in-vivo}$ is the MR resolution of the in-vivo brain data (0.5 mm isotropic), and t_m is the maximum cortical thickness (in percent). We adapted the width of the filter function for each area-specific model as the cortical thickness varies in different Brodmann areas. Values of absolute cortical thickness t_{BA} were taken from the tabulations of von Economo and Koskinas (1925). A width factor α was numerically determined to hold the following relation:

$$sinc(x) = sinc(\alpha \ width) = 0.5 \quad (8)$$

where α defines the Full-Width-Half-Maximum (FWHM = 0.5) according to the cortical thickness in individual Brodmann areas. In the filter function, we used the absolute value of a truncated cardinal sine function centred in the sampling window. The final filter function for resolution adaptation had the following form:

$$filter(x) = |sinc(\alpha(x - (t_m/2))|H(x). \quad (9)$$

$H(x)$ describes a Hamming window that was used to decrease the Gibbs phenomenon. We defined $H(x)$ as:

$$H(x) = (0.54 - 0.46(cos((2\pi x)/t_m)). \quad (10)$$

Finally, the modelled profiles $T_{1_{BA}}^{mod}$ were convolved with this filter function:

$$T_{1_{BA}}^{modMR}(x) = \left(T_{1_{BA}}^{mod} * filter\right)(x)dx \quad (11)$$

The convolution is defined in the range of relative cortical depth $d \in [0, 1]$. $T_{1_{BA}}^{modMR}$ is now a defined function of myelin-related T_1 values represented in MR space and MR resolution and has been modelled from known cytoarchitecture in individual Brodmann areas (BA) (see Fig. 3k). For consistency throughout the paper, we refer to the MR-resolved profiles as modelled MR profiles.

Measuring the similarity between area-specific models and in-vivo data

To facilitate comparisons between the area-specific models and empirical data, we defined a metric that estimates the similarity $P(T_1^{in-vivo} \in BA)$ of an in-vivo profile $T_1^{in-vivo}$ to belong to a certain Brodmann area (BA). For this purpose, the expected variance σ_{BA}^{modMR} of the modelled MR profiles in their corresponding location was estimated empirically from Dinse et al. (2013a). σ_{BA}^{modMR} determines the range of uncertainty (in milliseconds) by linearly interpolating empirical estimates of deviations in individual areas (see Table 1). Under the assumption that T_1 values, independently of their cortical depth, are normally distributed, we defined the probabilistic similarity $P(T_1^{in-vivo} \in BA)$ as a weighted Gaussian process with a prefactor $\delta = 1/2$ as:

$$P\left(T_1^{in-vivo} \in BA\right) \approx exp\left(-\delta \int_0^1 \frac{\left(T_1^{in-vivo}(x) - T_{1_{BA}}^{modMR}(x)\right)^2}{\sigma_{BA}^{modMR}(x)^2} dx\right). \quad (12)$$

Here, P compares how similar a single in-vivo profile $T_1^{in-vivo}$ of the cortex is to the modelled MR profile $T_{1_{BA}}^{modMR}$ in individual subjects. Similarity values range between 0 and 1, indicating low and high similarity.

Model validation in motor and somatosensory region

In order to validate this modelling approach using MRI, regions of interest (ROIs) in the left brain hemisphere were defined that correspond to primary and secondary areas of the motor and somatosensory region known as M1/S1 region. They specifically comprised Brodmann area (BA) 4, located in the posterior wall of the pre-central gyrus, Brodmann area 3b, located in the anterior wall of the post-central gyrus, Brodmann area 1, covering the gyral crown of the post-central gyrus, and Brodmann area 2, located in the posterior wall of the post-central gyrus. The location of these areas with respect to sulcal and gyral landmarks is consistent across subjects. All areas are located in a relatively small region of the brain, which allows a joint in-vivo and post-mortem study with ultra-high resolution 7 T MR brain imaging. The areas are anatomically contiguous or close neighbours, and they all have strong myelination levels. As a group, they stand out from neighbouring areas of the frontal and parietal lobe. However, the microstructural differences between these areas are subtle, thus accurately separating them is challenging for observer-independent parcellation schemes. It has been shown by Geyer et al. (1999) that there are changes in cytoarchitecture within Brodmann area 3, thus forming areas 3a in the sulcal fundus and 3b in the anterior wall of the post-central gyrus. Strictly speaking, BA 3a and 3b are not areas defined by Korbinian Brodmann, but were later introduced by Vogt and Vogt. We will continue using the Brodmann nomenclature as the tabulations of von Economo and Koskinas (1925) and the descriptions of Vogt and Vogt refer back to it.

Although the Vogts' division based on myeloarchitectonics is complex, Vogt (1910) suggested four main types of myeloarchitecture in the human cortex which are constant across brains. The chosen ROIs specifically exemplify each of these basic types. Brodmann area 3a, located at the fundus of the central sulcus between areas 4 and 3b, was not included in this analysis. Its myeloarchitecture has not been intensively studied and is thus not assignable to one of the four main types.

For all data sets acquired, ROIs were manually labelled in the left hemisphere within the abovementioned Brodmann areas. The labelling process was guided by accepted macro-anatomical landmarks (Grefkes et al., 2001; Geyer et al., 1999). All labels in in-vivo, ex-vivo, and histology data were used to derive mean profiles in each ROI and in each data modality. The mean profiles were compared to the area-specific models. Additionally, the manual labels on the 0.5 mm isotropic T_1 maps were used to validate the area-specific models on in-vivo data.

Research questions and experiments

The validation addresses the following major research questions:

- Q1 How well do individual empirical profiles derived from in-vivo data, i.e. in-vivo profiles, fit the respective modelled MR profiles (Eq. (11))?
- Q2 Can the area-specific models identify myeloarchitectonic signatures in different functional cortical areas in living subjects?
- Q3 How well do the area-specific modelled profiles (Eq. (6)) fit traditionally derived profiles, i.e. ex-vivo MRI and histology profiles?
- Q4 Which resolution is required to distinguish between cortical areas accurately and confidently using intracortical features measured with quantitative ultra-high resolution brain MRI?
- Q5 How helpful are measures such as the mean value and the shape of an individual in-vivo profile separately for the identification of specific human cortical areas?

The questions were answered using the here outlined corresponding experiments.

In Experiment 1, we compared the area-specific models quantitatively to in-vivo data. ROIs in the left hemispheric 0.5 mm T_1 map were defined and manually labelled. The samples covered between 1 and 2.5 cm^2 of the surface area in each ROI. Similarities P (Eq. (12)) were analysed by calculating a distribution of the similarity values in each ROI subject-wise. Similarity values P are expected to be high (approaching 1) in plausible locations, i.e. where in-vivo profiles belong to a certain Brodmann area, whereas in other regions the similarities are expected to be lower (approaching 0). Thus, the distribution of similarities P in a given ROI may vary with the model used. To provide comparable measures, we approximated the given distribution with a probability density function of a beta distribution with shape parameters α and β. Subject-wise, mode and standard deviation were estimated in each ROI. The mode defines the value at which the approximated beta distribution takes its maximum value, i.e. the value that is most likely to be represented by the similarities in each ROI. Computing the mode of a beta distribution requires that the parameters α and β are greater 1. If the approximation yielded values of $(\alpha, \beta) < 1$, the distribution of similarity values was skewed too much to either 0 or 1 such that the calculated beta distribution became asymptotic. In these extreme cases, the mode of the distribution (respectively the standard deviation) cannot be computed and we therefore assigned 0 to the mode and standard deviation. This validation was performed on a single-subject as well as a group-average basis.

Experiment 2 addresses the question of how well the models perform in one and the same ROI. We therefore computed for each location in the human cortex the similarity values across the area-specific models and marked the area-specific model with the highest value at that location.

In Experiment 3, we qualitatively compared ex-vivo and histology profiles to modelled and in-vivo profiles in order to analyse the relationship and likely similar trends in profile shapes. All profiles were transformed into a normalised space with arbitrary units to match the different contrasts and resolutions of the different data origins. The objective of this validation is to study the apparent laminar myelination change in each Brodmann area, given the different scales of resolution.

The analysis of Experiment 4 was performed among the different area-specific modelled profiles (Eq. (6)). The profiles were transformed into different scales of resolution using the filter function in Eq. (9). In order to change the resolution at each scale, *resMR*, i.e. the parameter defining the resolution, was changed in 50 μm steps starting at a resolution of 1 μm and then increasing up to 1 mm. Waehnert et al. (2013a) used profiles originating from T_1 maps of different resolutions. They found that the standard deviation decreases at higher resolution. Here, the standard deviation was simulated to be smaller at a higher resolution and to be slightly larger at a lower resolution. A theoretical similarity P_t was calculated between the different resampled area-specific models at each scale of resolution. For application to in-vivo data, the modelled MR profiles were downsampled. Here, the modelled profiles were used at their original cell size resolution to reduce sampling artefacts when observing changes in profile shape.

Experiment 5 deals with a more general question considering the information content of in-vivo cortical profiles. To show to what extent both a profile's mean and its shape matter, we performed additional experiments using these two measures separately in Eq. (12). In the mean-experiment, the mean T_1 value of the modelled MR profile was compared to the mean T_1 value of an individual in-vivo profile. The mean T_1 value itself was simply computed as the average across the profile's cortical depth. In the shape-experiment, the mean distance between the profiles was calculated through cortical depth. To allow comparisons of shape only, we demeaned the modelled MR profile in advance by shifting it to the mean T_1 value of the empirical profile.

Software

All data were processed using the CBS Tools software package integrated into the MIPAV and JIST framework (Bazin et al., 2013; Lucas et al., 2010). The CBS Tools are freely available for download from the Max Planck Institute for Human Cognitive and Brain Sciences website: http://www.cbs.mpg.de/institute/software/cbs-hrt/index.html and from NITRC: http://www.nitrc.org/projects/cbs-tools/.

Results

T_1 fMaps and cortical in-vivo profiles

Glasser and Van Essen (2011) have already presented lower resolution (1 mm) maps describing mean cortical myelin content. Bridge and Clare (2006) and Walters et al. (2003, 2007) earlier showed microstructural detail in individual cortical profiles. As the spatial resolution of the T_1 maps improves, finer details of myeloarchitecture are revealed. Cortical profiles derived from 0.5 mm T_1 maps clearly carry more information than the mean of a profile alone.

The T_1 maps used in this study are able to capture finer details of myeloarchitecture than maps describing mean cortical myelin content presented by Glasser and Van Essen (2011). The T_1 maps used provide contrast differences between primary/secondary areas (lower T_1 values) and other less heavily myelinated areas (higher T_1 values). Frontal and parietal regions clearly differ in contrast. The difference in myelination between the motor region M1 and the somatosensory region S1 is visible in Fig. 2A and in the mean experiment shown in Fig. 7 (second column). With the isotropic ultra-high resolution of 0.5 mm, the in-vivo data reveal medio-lateral variation of T_1 values in the primary motor area M1. Within M1, a location with even darker T_1 values (encircled in white in Fig. 2A) can be detected that corresponds to the motor hand knob known to be the most strongly myelinated part of the primary motor region. These observations agree with historic maps representing cytoarchitectural distributions (Brodmann, 1909;von Economo and Koskinas, 1925) as well as myeloarchitecture

(Vogt and Vogt, 1919a,b; Hopf, 1955, 1956; Hopf and Vitzthum, 1957; Smith, 1907).

The (T_1) values of profiles in Brodmann area 4 are very low (indicating higher myelination) for each individual imaging modality (see Fig. 6). Area 4 has myelinated tangential fibres in upper cortical layers (Vogt and Vogt, 1919a,b). These additionally cause a higher degree of myelination in the upper cortical layers of area 4 than in the corresponding layers of area 3b. The described myelination translates into expectations for the T_1 profile values. Low T_1 values (in ms) are found in deeper cortical layers of both areas 4 and 3b as shown in the in-vivo average profiles of areas 4 and 3b, presented in Fig. 4 (first column). The T_1 values for upper cortical layers of areas 4 and 3b, however, differ. The cortical profiles derived from our T_1 maps clearly display this difference. The T_1 values in the upper layers of area 4 are much lower than the corresponding T_1 values in area 3b.

Comparing models to in-vivo brain data (Exp. 1, 2)

Fig. 4 illustrates the results corresponding to Experiment 1 from a single subject. The strongly alternating profile shape of the modelled profiles (Fig. 4, left column, magenta, dashed) represents the underlying laminar myeloarchitectonic patterns at cell size resolution. Higher myelination is associated with lower T_1 values. The transparent bands of the in-vivo profiles and modelled MR profiles represent the standard deviation. The dips visible in the profiles correspond to higher myelinated intracortical structures. The area-specific MR models (shown in red) correspond well to in-vivo profiles. When the resolution is decreased, the area-specific modelled MR profiles reveal less of their characteristic structure as compared with the modelled profiles. Given a certain resolution, both the in-vivo and modelled MR profiles are different across the areas. The loss of structural features in the area-specific models with decreasing resolution is depicted in Fig. 6B.

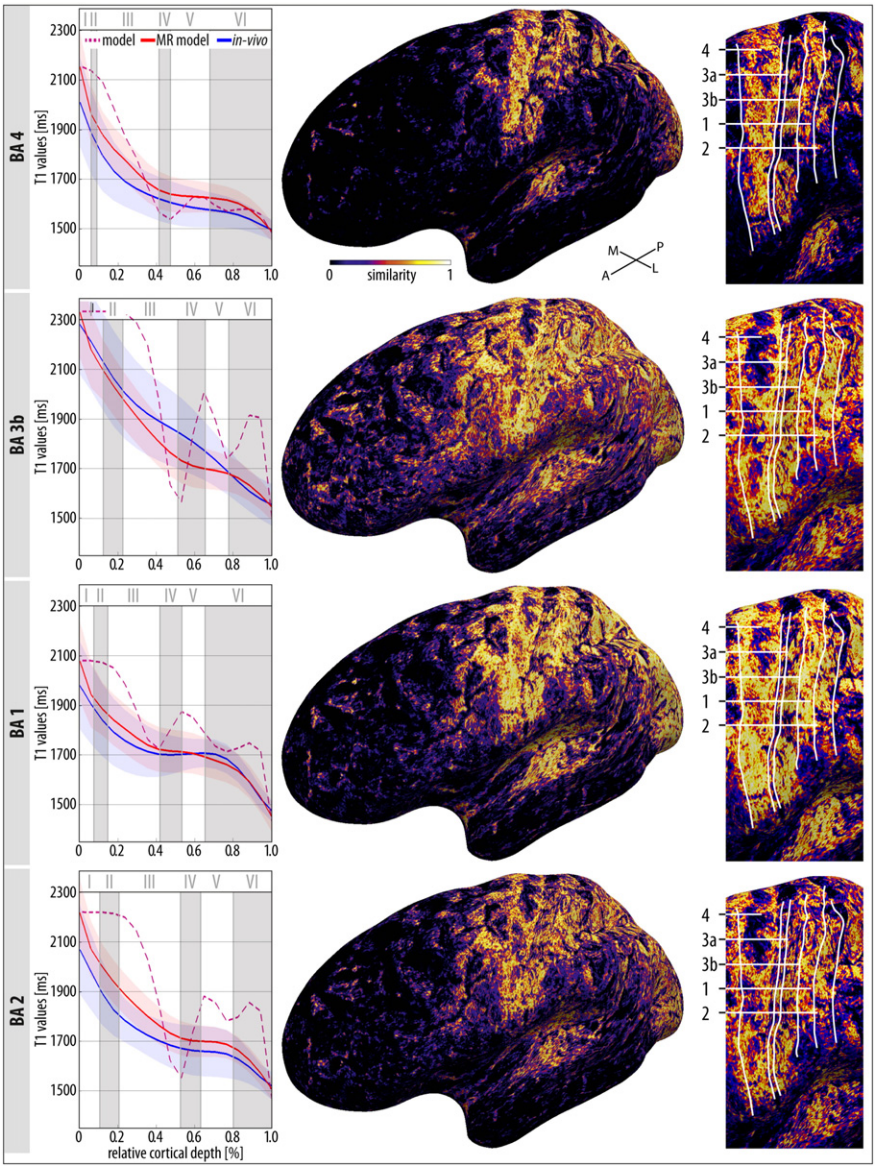

Fig. 4. Application of the presented model to a single subject is shown. Left column: Area-specific modelled profiles (magenta, dashed) are compared against mean in-vivo profiles (blue, solid) and modelled MR profiles (red, solid) in one individual subject. Lower T_1 values represent higher myelin concentration. The transparent bands represent the modelled and measured standard deviations. The area-specific MR models correspond well with the mean in-vivo profiles. Middle column: Maps of a single subject's similarity values are shown on the cortical surface. Right column: Enlargements of the considered ROIs. The zoomed-in pictures show higher intra-ROI similarities when there is a match between a model and the respective Brodmann area. When the model and the location of an area do not correspond, the results show smaller similarities and/or inconsistent patterns.

Table 2
A summary of the quantitative comparisons between area-specific MR models and in-vivo profiles. The mode and standard deviations (given in brackets) were computed from the estimated beta distribution of the underlying similarity values in each ROI. The diagonal boxes (blue) describe a given model at its corresponding location. Anatomically neighbouring areas are highlighted in yellow.

		Group average				Single subject			
	BAs	4	3b	1	2	4	3b	1	2
Modelled profiles	4	0.75 (0.207)	0.0 (0.0)	0.0 (0.0)	0.0 (0.0)	0.619 (0.219)	0.0 (0.0)	0.521 (0.217)	0.636 (0.217)
	3b	0.333 (0.262)	0.718 (0.193)	0.0 (0.0)	0.750 (0.198)	0.05 (0.199)	0.611 (0.192)	0.461 (0.211)	0.434 (0.180)
	1	0.777 (0.181)	0.0 (0.0)	0.941 (0.210)	0.937 (0.214)	0.5 (0.244)	0.0 (0.0)	0.84 (0.162)	0.678 (0.164)
	2	0.0 (0.0)	0.0 (0.0)	0.0 (0.0)	0.687 (0.299)	0.0 (0.0)	0.0 (0.0)	0.45 (0.223)	0.379 (0.203)

In Fig. 4, second column, the similarities *P* are mapped onto the cortical surface for each model indicating high similarity (coded bright yellow) or low similarity (coded bluish to black). In general, the area-specific MR models show higher similarities in primary cortical areas, but not in areas located at the frontal lobe. Some areas are highlighted in the parietal lobe and the occipital pole. These structures are more strongly myelinated than the prefrontal brain, but not as strongly myelinated as primary areas, which confirms previous research (Vogt and Vogt, 1919a,b; Hopf, 1955, 1956; Hopf and Vitzthum, 1957).

The right column in Fig. 4 shows zoomed-in results, focussing on the defined ROIs, of the same subject. The model of Brodmann area 4 shows clear results. Higher similarities (shown in yellow) are consistently distributed in location BA 4, whereas the similarities get smaller and the distribution pattern gets more patchy in other areas. The results are similar for the model of Brodmann area 3b. Neighbouring locations such as areas 4 and 1 show lower similarity values. The model of Brodmann area 1 shows lower similarity values in location of area 3b and area 2. The model of Brodmann area 1 has high similarity values in location of area 4. The model of Brodmann area 2 does not stand out well. The discrimination between the four areas may be rather poor. In general, the similarities are higher in plausible locations (model and area match) while they are smaller in directly neighbouring areas. The individual models reveal smaller similarities and/or inconsistent patterns (small different clusters) when the location of the Brodmann area and the area-specific model do not match.

The quantitative comparisons between area-specific MR models and in-vivo profiles are summarised in Table 2. Given a certain model, it mostly performs best in its corresponding location (diagonal, coloured blue) and outperforms directly neighbouring areas (coloured yellow). This is true for individual subjects as well as the group data. When the distribution of similarity values was skewed to 0 or 1, the approximated beta distribution becomes asymptotic. The mode and standard deviation cannot be estimated and were set to 0. The distribution of the area-specific similarities (blue) and the estimated beta distributions (red) are additionally shown in Fig. 8 in the Supplementary material. Graphs are illustrated for the group-average and for the single subject shown in Fig. 4.

Brodmann area 2 is an exception (compare with Fig. 4, right column). Here, the underlying data is highly variable, which arises from imaging artefacts as well as small segmentation errors. The T_1 maps show ringing artefacts resulting from motion of the subjects. A ringing effect is already respected in our modelling approach, too (see Fig. 3h). The artefacts appear in the back of the brain and encompass the post-central gyrus but barely reach more into anterior regions, i.e. the central sulcus (see Fig. 9 in the Supplementary material). The ringing artefacts do thus not affect area 3b very much and area 4 is even less affected. The effects usually intrude the imaging data in location of the cortical surface up to a depth of 1.5 cm. Therefore, all remaining areas of interest in the post-central gyrus, i.e. areas 1 and 2, show these small effects. Its influence on the final modelling result is different for the two areas, because the influence depends on the orientation and position of the area as well as its cortical thickness. The ringing artefacts appear parallel in the cortex of area 1 and orthogonally in the cortex of area 2. Given the different cortical thicknesses of these locations with area 1 being thick at the gyral crown and area 2 being relatively thin in the sulcal wall, this ringing significantly affects the cortical segmentation result, and leads to larger inaccuracies when calculating the cortical profiles. In area 1, segmentation errors occur rarely, and their effects average out when the cortical profiles are calculated. In area 2, however, the segmentation of the boundary surfaces is affected by the artefact, which in turn impairs the quality of the cortical profiles. Comparing these corrupted profiles with an area-specific MR model leads to low similarity values, although intracortical contrast remains visible in this area.

Blood vessels are another issue. With the new resolution, blood vessels with a diameter of 0.5 mm can be captured. Thus, their influence appears even stronger compared to standardly used MRI data. Segmentation errors due to blood vessels occur in various regions of the cortex. Here, the effects of segmentation errors due to blood vessels are most prominent in area 2, where the anterior parietal (or post-central sulcal) artery extends medially into the post-central sulcus. Branches of the paracentral artery reach laterally into the central sulcus region. These extensions usually follow the gyral crowns and their branches reach into the sulcal basins. Vessels on the crown have a diameter larger than the imaging resolution and are well discriminated with the segmentation methods used. However, their branches have a diameter close to or even smaller than the imaging resolution and are sometimes misclassified as belonging to grey matter. All these effects influence the performance of the model of Brodmann area 2. In the future, better methods have to be developed to capture the vessels' characteristics and to reduce segmentation errors.

From the aforementioned analysis, the question arises if the individual models are able to capture area-specific signatures. Fig. 5 depicts a single-subject surface on which we mapped at each location the model with the highest similarity value. Patterns of models 4, 3b, and 1 overlap with the corresponding locations of these areas. In location of Brodmann area 4, the model of area 1 is slightly present and vice versa. These two areas are very similar and hard to distinguish. The similarity values of the model of Brodmann area 2 are smaller than similarity values from other models. Thus, there is no obvious cluster representing the location of Brodmann area 2.

Comparing models to post-mortem brain data (Exp. 3)

Fig. 6, first row, shows a comparison between group-average in-vivo profiles (dark blue), ex-vivo profiles (light blue), histology profiles (green), and a group-average of the area-specific models (red). The comparison is shown for each ROI. All profiles were transformed into a normalised space, with arbitrary units ranging between 0 and 1 to match different contrasts and resolutions of the different data origins. Lower values are again associated with higher myelin concentration. We hypothesise that profiles with similar resolution should have similar profile shapes. Indeed, the modelled (red) and histology profiles (green) are qualitatively similar. They show the same trends at the same locations although the intensity of change is not the same. The ex-vivo profiles (light blue) preserve some shape characteristics, but striking features visible in the modelled and histology profiles are weakly noticeable here due to limiting resolution effects. The in-vivo profiles show less characteristic structure, but follow the general trend of the other profiles.

Resolution experiment (Exp. 4)

Area-specific models at different scales of resolution are shown in Fig. 6, second row. The pictures illustrate the effect of decreasing resolution on profile shape characteristics. Strong shape features, such as

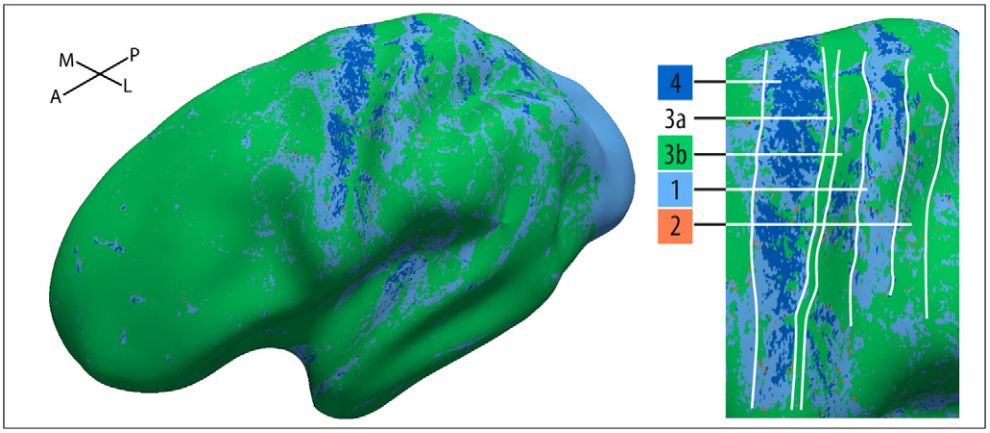

Fig. 5. The images depict at each location the area-specific model with the highest similarity value. Surface and zoom-in on ROIs are shown for the single subject presented in Fig. 4. Models reveal area-specific signatures. There is no obvious cluster representing the location of Brodmann area 2 as similarity values of the other models were higher.

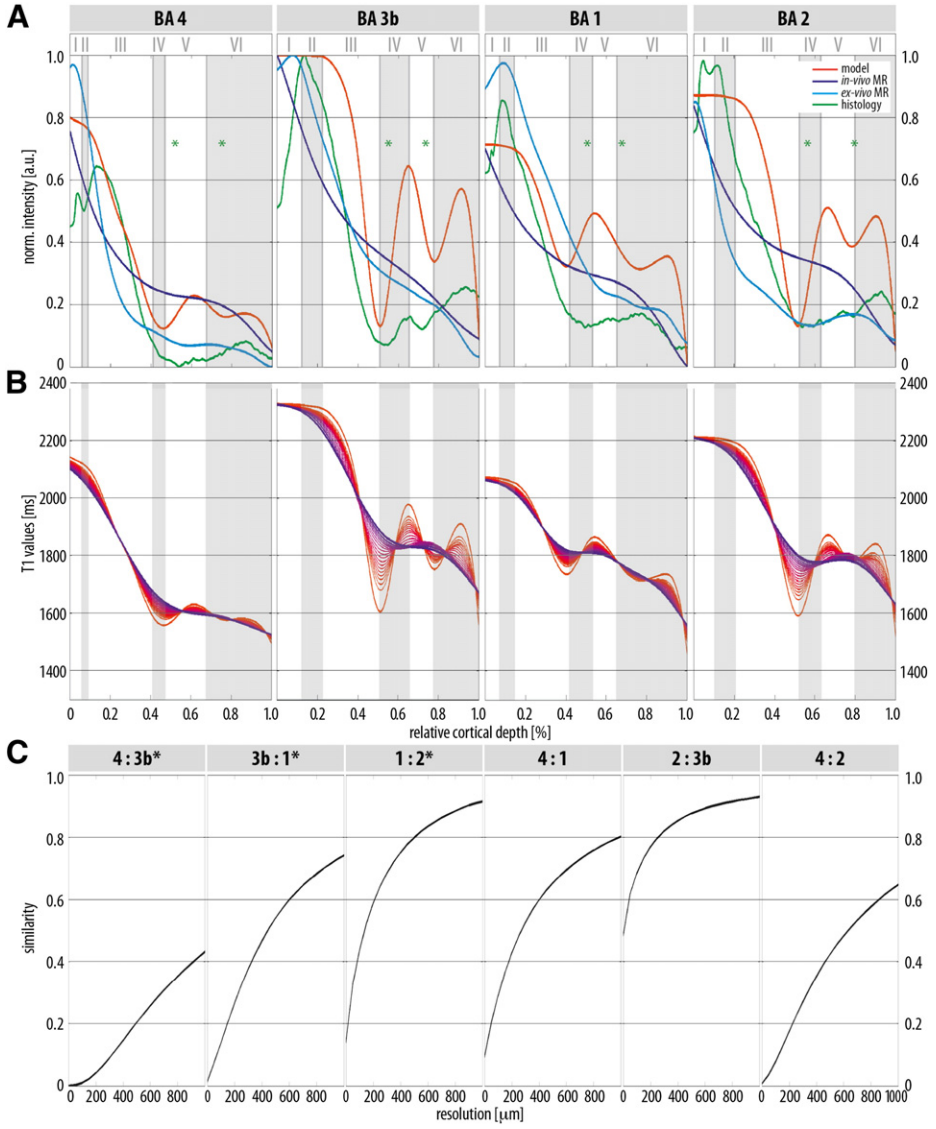

Fig. 6. A) A comparison between area-specific models and group-average in-vivo, ex-vivo, and histology profiles is shown. The myelination pattern agrees between the area-specific model and histology. The dips present in the area-specific and histology profiles depict Baillarger banding. The dips visible in the histology profiles (marked with asterisk) are similar to those of the area-specific models. The differences in myelination are located at similar relative cortical depths for different imaging techniques in each Brodmann area. In general, the myelination trend is preserved in ex-vivo and in-vivo profiles. B) Modelled profiles were transformed into different scales of resolution starting at 1 µm (red) and increasing up to 1 mm (blue). As resolution is coarsened, salient features disappear quickly. Even at lower resolutions, profiles at the same scale are different across Brodmann areas. C) Theoretical performance is shown on how similar the area-specific models are at different resolutions.

turning points along the profile, vanish quickly with decreasing resolution. At 0.4–0.5 mm resolution, striking features become weaker. However, at a given resolution the profile shapes in each area are noticeably different, an observation which has already been pointed out when comparing in-vivo and modelled MR profiles in Fig. 4. Thus, the following question arises: which resolution is needed to distinguish between profiles originating from different cortical areas?

The bottom row of Fig. 6 depicts the theoretical similarity *Pt* for directly neighbouring areas 4 vs. 3b, 3b vs. 1, and 1 vs. 2 (all marked with an *) as well as not directly neighbouring areas 4 vs. 1, 2 vs. 3b, and 4 vs. 2. The similarity is illustrated according to decreasing resolution. The challenging task for this approach is to distinguish between neighbouring areas. The similarity plots show that Brodmann areas 4 and 3b can be well discriminated even at lower resolution. It is easier to distinguish Brodmann area 3b from 1 than Brodmann area 1 from 2. Brodmann areas 1 and 2 are similar at higher resolution, too. In the case of non-neighbouring areas, Brodmann areas 2 and 3b are the most similar, directly followed by Brodmann areas 4 and 1. Brodmann areas 4 and 2 are the most dissimilar areas. In general, the slope of the similarity curve is high, given high resolution (except Brodmann areas 4 vs. 3b and 4 vs. 2), and starts to become smaller after 800 μm. At our working resolution of 0.5 mm, neighbouring Brodmann areas 4 and 3b are well discernible. However, Brodmann area 2 cannot be reliably separated from other areas. Brodmann areas 4 and 1 are hard to distinguish. The outcome of the theoretical experiment here confirms results in Figs. 4 and 5, and Table 2.

Profile attributes: mean and shape (Exp. 5)

Finally, we investigated the information contributed separately by the mean and the shape of an individual in-vivo profile. In Fig. 7, first row, we schematically depict the different measures considered (from left to right): our presented approach, the mean-experiment, and the shape-experiment.

For comparison, the first column depicts the results of our approach on a cortical surface (as shown in Fig. 4). The second column shows results of the mean-experiment. The third column shows results of the shape-experiment.

In normal adult human brain, area 4 is the most highly myelinated cortical area. Profiles found in this location have very low T_1 values, leading to very low mean values and large differences in profile shape when compared to profiles derived from other regions in the cortex. Therefore, using Eq. (12) with only the mean T_1 value of a profile results in high similarities in locations of area 4 and low similarities in other

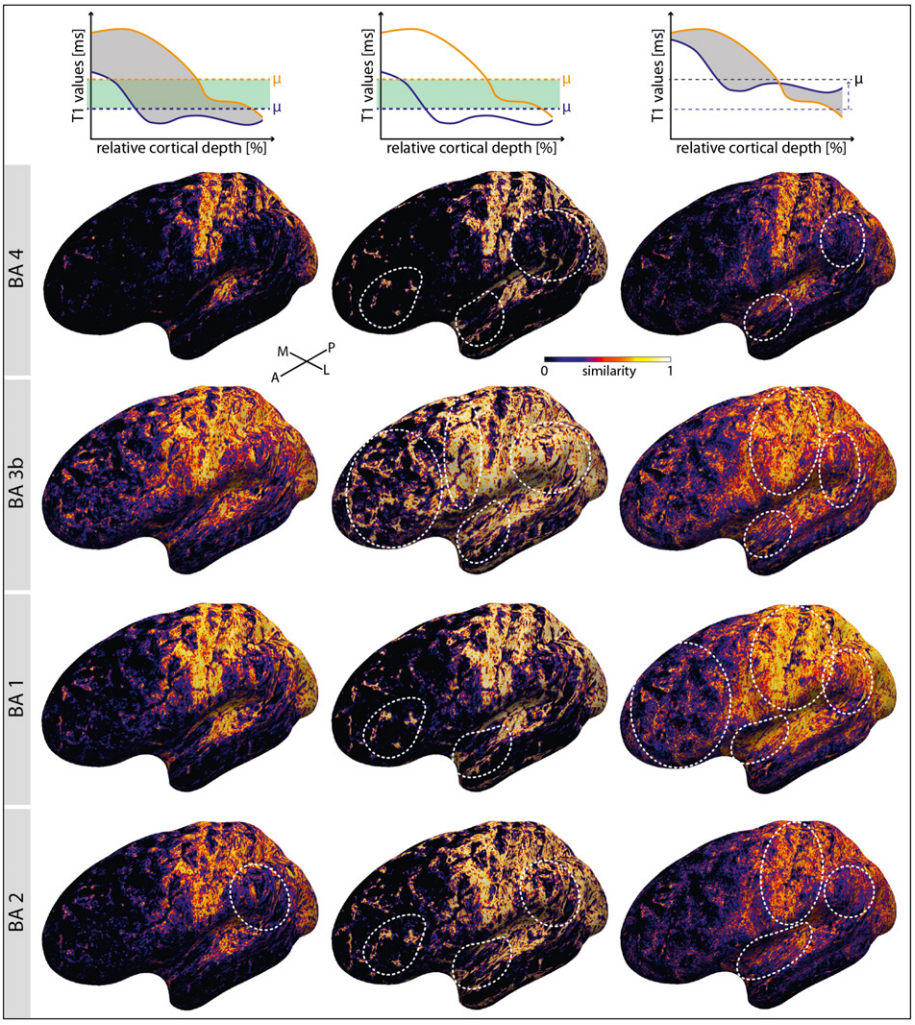

Fig. 7. Additional experiments depicting the comparison between the presented approach and the mean- and the shape-experiments (middle and right column). The mean-experiment yields an almost binary result in which frontal, parietal, and temporal regions are equally similar. The shape-experiment provides even less distinction in the ROIs. Differences are encircled. The performance is best when using the mean and shape in a combined setup as presented in this work. It leads to high similarities when location and model match and low similarities in the case of a mismatch.

locations. Therefore, the three surfaces corresponding to the model of area 4 in Fig. 7 reveal fewer differences when comparing the effects between our approach, the mean- and the shape-experiments.

In each case, the areas are best discriminated when using our approach which not solely depends on mean T_1 value but incorporates shape differences, too.

The mean-experiment presented in Fig. 7 for Brodmann areas 3b and 1 shows that using the mean T_1 value of a profile alone is insufficient. Locations across the cortex are categorised as either very similar or very different, with no intermediate variation. Frontal, temporal, and parietal parts appear to be equally similar when applying the models of area 3b and area 1. A similar pattern can be observed for the shape-experiment when using the models of Brodmann areas 3b and 1. Here, the selected regions of interest are poorly distinguished.

In many locations across the cortex, cortical profiles reveal lower T_1 values in upper cortical layers and, at the same time, higher T_1 values (less myelin) in lower cortical layers. Therefore, if we compare the mean T_1 value of these profiles, there is no noticeable difference. Hence, profiles from different locations in the cortex appear similar when using the mean T_1 value alone, although their underlying real microstructure may be different.

The shape-experiment presented in Fig. 7 shows that using the mean distance between profile shapes is insufficient, too. The shapes may differ due to higher or lower T_1 values in upper or lower cortical layers. The total shape difference through cortical depth may be the same in different locations across the cortex, and, thus, the similarities differ not much. Here, the same conclusion as in the mean-experiment can be drawn: profiles from different locations in the cortex appear similar when using the shape only, although the underlying microstructure may be different.

The effects are less convincing when the model of Brodmann area 2 is applied. Possible reasons for the failure of the model of Brodmann area 2 were discussed previously in Section 3.2.

Myeloarchitecture and area-specific results

There is a close relation between the cytoarchitecture and myeloarchitecture. The four myeloarchitectonic types present in the cortex are depicted in Fig. 1B (reproduced from Hopf (1968, 1969)). Here, we relate the results from the experiments to descriptions of myeloarchitecture.

The primary motor cortex M1 (Brodmann area 4) is reported to be of astriate type (Hopf, 1967). The (T_1) values of profiles in Brodmann area 4 are very low (indicating higher myelination) for each individual imaging modality (Fig. 6A). The minima in the area-specific modelled profile (red) have the same strength. The difference in amplitude between minima and maxima is small. Histological data confirms this difference in myelination (see Fig. 6A). Due to small artefacts occurring close to the pre- and post-central gyral crowns in the ex-vivo MR data, the T_1 values in area 4 are increased in the ex-vivo profile, i.e. the difference is less apparent.

The primary somatosensory cortex S1 (Brodmann area 3b) is described to be of bistriate type, which is supported by the profile shape of the area-specific model of Brodmann area 3b (Fig. 6A). The outer band seems to be stronger myelinated. The area-specific model of Brodmann area 3b shows a deeper turning point (higher myelination) in layer IV in which the outer band of Baillarger is located. The same trend is visible in the histology profile of this area.

Brodmann area 1 (crown of the post-central gyrus) is considered to be of unitostriate type (inner and outer bands of Baillarger fuse together). Area 1 has equally dense myelinated layers. In Fig. 6A, all profiles of Brodmann area 1 appear on average less myelinated (higher T_1 values) in lower cortical layers IV–VI compared to the graphs of Brodmann areas 4 and 3b. The minima in the area-specific model of Brodmann area 1 have the same depth in terms of T_1 values. The difference in amplitude between minima and maxima is small. The histology profile almost stagnates in the deeper cortical layers with almost no difference between the two bands of Baillarger being visible. Thus, Hopf's definition of Brodmann area 1 being of unitostriate type with equally dense myelinated layers is replicated here.

Brodmann area 2 (located in the posterior wall of the post-central gyrus) is, according to Hopf (1968, 1969), of unistriate type with an outer band of Baillarger being more pronounced. The area-specific model (Fig. 6A) clearly indicates higher myelination in the location of the outer band. The difference compared to the inner band is large. In the histology profile as well as in the ex-vivo profile there is a clear minimum in location of the two Baillarger bands. However, the separation into two bands is only visible in the histology profile. The data fit Hopf's definition of a unistriate type with a pronounced outer band.

Discussion and conclusion

In contrast to cytoarchitecture, established computational parcellation methods based on myeloarchitecture do not exist yet. In this work, we established a cytoarchitectonically-driven model that is able to provide laminar area-specific estimates of myelin visible in quantitative T_1 maps. The key contribution of this work is to lead Hellwig (1993) conceptual approach to a practical application to MRI data. As this work presented here is the first known in-vivo application of Hellwig (1993) method, the model can only be seen as a starting point for further investigations of cortical myelin distribution. The model is validated by quantitatively analysing it on in-vivo data and comparing it to classically-derived information from post-mortem material. The visual patterns are different from each other and appear to be area-specific.

Modelling aspects

In general, Hellwig (1993) model depends on many assumptions and parameters which he derived from the work by Sanides (1962) and Braitenberg (1962). Sanides (1962) found that “the total amount of myelin in a given area is positively correlated to the cell body sizes in this area” and “in regions where a cortical layer containing large cell bodies is situated above a layer in which the neurons are smaller or less densely packed, a horizontal stripe of myelinated fibres appears above a layer where horizontal fibres are less evident”.

Hellwig drew a conclusion from Sanides' first finding and simplified it to his first assumption: large neurons contribute more to intracortical myelin content than small ones. In this work, we modelled this relation as a sigmoid function (see Eq. (1) in Section 2.3.1).

Sanides' second finding has been further investigated by Braitenberg (1962, 1974) who tried to explain these phenomena with the help of horizontal myelinated fibres. These fibres correspond to axonal collaterals of pyramidal cells. As observed in Golgi preparations, the majority of these axonal collaterals branch off the descending main axon 200–300 μm below the cell body. The pyramidal cells, most conspicuous in cytoarchitectonic layers III and V of Nissl preparations, thus produce two maxima of horizontal fibres. These maxima, shifted downwards relative to layers III and V by 200–300 μm, account for the two stripes of Baillarger (see Fig. 1A for comparison). Braitenberg's explanation was supported by several other studies (Le Gros Clark and Sunderland, 1939; Creutzfeldt et al., 1977; Gatter et al., 1978; Fisken et al., 1975; Colonnier and Sas, 1978). Indeed, there is a structural mismatch between cyto- and myeloarchitectonic layers. The axonal collaterals of larger cells (especially pyramidal cells in cytoarchitectonic layers IIIb and V) form fibre bundles in deeper myeloarchitectonic layers (see in Fig. 1A, compare cytoarchitectonic layer IIIb and V to myeloarchitectonic layer 4 and 5b). Quantitative measures on the distribution of such axonal collaterals were provided by Paldino and Harth (1977) and also found application in our work.

To compare his area-specific models to myelin preparations, Hellwig (1993) simply linearly transformed the profiles into grey values. Values

located at the pial surface represented 0% myelin, values at the WM interface corresponded to 100% myelin. This assumption is valid only for a qualitative comparison. However, it is not in agreement with classical works by Braitenberg (1962) and Hopf (1967, 1968, 1969, 1970). Vogt and Vogt (1919a) and also von Economo and Koskinas (1925) pointed out that there are variations in myelin in pial surface as well as towards the WM boundary surface. Dinse et al. (2013a) and Tardif et al. (2013) recently showed that the myelin distribution in different cortical depths varies between different cortical areas when using in-vivo high-resolution quantitative T_1 maps.

In addition, partial voluming is a problem in MRI at any resolution, but becomes particularly severe in tightly folded cortical sulci. The processing pipeline employed (Bazin et al., 2013) handled most types of partial voluming robustly. However, in locations where neighbouring cortical folds were almost in contact, CSF image intensities have a high spatial dependence and differ quite strongly compared to other locations.

To correct for the myelin-related variability in individual areas as well as the partial volume effects, we introduced the area-specific estimates $\hat{e}_{wm}$ and $\hat{e}_{csf}$ in Eqs. (4) and (5) (see Table 1). Partial volume effects become more severe when adjacent tissues such as GM and CSF differ greatly in T_1 value. Profiles of the cortex have a greater variance at the GM/CSF boundary than at the WM/GM boundary. Thus, the estimates $\hat{e}_{csf}$ at the GM/CSF interface have a larger spread compared to the estimates $\hat{e}_{wm}$ at the WM/GM interface.

The positive values of $\hat{e}$ have two functions: on the one hand, they decrease the T_1 values to model higher myelin concentration. At the WM/GM boundary it yields a poor discriminative power between the tissue types. This is specifically true for areas 4 and 1. Area 3b was described to have the best separation between WM/GM and GM/CSF (Vogt and Vogt, 1919a; von Economo and Koskinas, 1925). Ideally, area 4 should have the highest estimate $\hat{e}_{wm}$ to model strongest myelin concentration. From Han et al. (2003) and Bazin et al. (2013) it is known that the WM/GM boundary may get stuck in WM in gyral crowns yielding T_1 values similar to WM. Therefore, $\hat{e}_{wm}$ is highest for area 1 rather than area 4. On the other hand, positive values of $\hat{e}$ help to model PV artefacts at GM/CSF boundary. Larger values of $\hat{e}_{csf}$ model higher myelin concentration in upper cortical layers by decreasing the T_1 values again. But a higher degree in myelination in upper cortical layers also yields a better separation in the segmentation of GM and CSF. As described above, PV artefacts are severe in tightly folded sulci. In these structures also the separation of tissues is hard to define during the segmentation process. In the scope of this work, areas 4 and 3b were mostly affected. Ideally, area 4 has the lowest T_1 values in upper cortical layers. But due to its location in the central sulcus, PV effects artificially increase the T_1 values at the GM/CSF boundary. Therefore, $\hat{e}_{csf}$ of area 4 is not the highest. In locations of gyral crowns, such as in the case of area 1, PV is less strong. The segmentation at the GM/CSF is more accurate. With less PV artefacts being present and a myelin concentration in upper cortical layers comparable to area 4, area 1 has the highest estimate $\hat{e}_{csf}$ at the GM/CSF boundary.

In general, myelination is higher at the WM/GM boundary than at the GM/CSF boundary. This has already been shown using classical histology (Hopf, 1968, 1969, 1970). Due to the Baillarger banding, the variation of myelin concentration is higher in lower cortical layers than in upper cortical layers. Now, a comparison between cortical MRI profiles and classical histology profiles, as presented by Hopf (1967) or Braitenberg (1962), may lead to confusion. In MRI, the GM/CSF boundary is highly partial-volumed, i.e. the T_1 values in the cortex are distorted by much higher T_1 values found in CSF, which may give rise to the impression that the myelin concentration changes more strongly in upper cortical layers. Rather than expecting an almost stagnating profile shape towards the pial surface, in-vivo and ex-vivo MR profiles show a high increase of T_1 values.

Limitations considering the area-specific modelling

Possible sources of uncertainty within the models itself may be different cell densities or cell sizes in Brodmann areas, given that the numbers can only be derived from post-mortem material. The model is based on the assumption that larger cells contribute more to the myelin concentration, as their myelinated axonal collaterals carry more myelin. This relationship is modelled using a sigmoidal function. The myelin concentration varies not only in location of the bands of Baillarger but at the boundary between WM/GM as well as between GM/CSF based on incoming radial or tangential fibres in the pial surface of the cortex. This variability needs to be further investigated in-vivo. In addition, it is necessary to determine and define changes and variability of the cellular composition depending on age, gender, brain development, or disease. Age has a tremendous effect on brain structure and function. With increasing age, cells die and myelinated fibres change, and this process may be accelerated in disease states (Peters, 2002). Cortical myelination is well known to continue into the third decade of life but gradually reduces with advancing age (Lintl and Braak, 1983). Age may correlate with regionally specific decreases in myelin content, changes in iron (Hallgren and Sourander, 1958) and water content and ultimately with brain atrophy (Callaghan et al., 2014).

In terms of T_1 values, there is an increasing interest in the neuroscience community to what extent other factors, such as iron or susceptibility, may influence the contrast of the T_1 maps. The work of Stüber et al. (2014) suggests that, within the cortex, the value of T_1 is dominated by myelin content. Incorporating new findings may further improve the performance of the presented approach.

The T_1 maps used in this study are comparatively new. In order to explore the modelling approach in a focused way, we kept several parameters constant across subjects, such as cortical thickness and values of T_1 for WM and CSF. These were supported by previous literature. With more T_1 maps acquired and analysed, it will be possible to replace tissue values taken from Rooney et al. (2007) with reliable values derived from these new T_1 maps. The same applies to cortical thickness values which can be replaced by more subject-specific mean cortical thickness values. In addition, newer cytoarchitectural data are needed describing average measures on cell size, cell number, and layer thickness, but specifically providing variances for each of the measures.

Limitations considering in-vivo mri acquisition and data segmentation

In the group data some subjects lack overall consistency in data quality. Small motion artefacts and image artefacts may strongly affect the results. Head motion typically has a global effect, decreasing the similarity values for each model. This problem can be overcome with adequate methods for removing motion artefacts, such as prospective motion correction (Schulz et al., 2012). In contrast, image artefacts may have local effects and lead to better performance of a given area-specific model in other locations, e.g. the model of Brodmann area 4 may perform better in the location of area 1 (and vice versa) and the discrimination between area 1 and 2 may be impaired. Future analyses will include more data to better characterise and control image artefacts, and thus increase the performance of the approach. Advanced cortical registration techniques may help to increase the robustness and reproducibility of the results (Tardif et al., 2013; Robinson et al., 2013). In addition, the approach presented using T_1 maps could be usefully combined with other data such as probabilistic maps or gyral maps, and even task fMRI data to further understand the relationship between structure and function in the human brain.

Another limitation of the approach is the current in-vivo image spatial resolution, which is constrained by the scan duration. Below a cortical thickness of 1.5 mm, the profiles generated from the empirical in-vivo data carry a smaller amount of information compared with the modelled MR profiles. In locations of small segmentation errors (oversegmentation) the empirical profiles may still carry enough

information which is skewed into the profile's cortical depth. Important myelin-related intracortical features of the empirical profile are thus not well aligned with the features in the corresponding model affecting single subject as well as the group average results. Brodmann area 2 is the most inconsistent structure of the ROIs. Anatomical differences occurring in the individual brains may play a certain role, too. In some subjects the dura mater is almost in contact with the brain matter, other subjects have CSF between brain matter and dura mater. In these locations, the T_1 values at the CSF boundary surface have a high spatial dependence leading to strong partial voluming effects. Hence, T_1 values at the CSF boundary vary depending on their location in the folded cortex and between subjects. In future work, more sophisticated modelling of CSF variability is likely to be needed.

In general, the practical performance of the presented model is in agreement with the theoretically computed performance given in Fig. 6C. It appears that a resolution as high as 0.3 mm will be required to reliably distinguish the cortical areas solely based on intracortical features. At 0.3 mm the similarity values between neighbouring (4 vs. 3b, 3b vs. 1) and non-neighbouring areas (4 vs. 1, 4 vs. 2) are mostly below 0.5, thus, areas can more likely be distinguished. The theoretical performance calculations show that the bands of Baillarger, their location in cortical depth, and their degree of myelination are important. In addition, the experiments shown in Fig. 7 indicate that mean and shape in a combined setup perform best compared to mean or shape alone. Average cortical myelin maps effectively depict primary areas even at lower resolution. But T_1 maps at 0.5 mm isotropic resolution and their derived profiles' mean and shape information bring further discriminative power when distinguishing between cortical areas. Spatial or geometrical priors, such as curvature, may be necessary in order to precisely distinguish between Brodmann areas 1 and 2 and between Brodmann areas 2 and 3b.

Limitations considering comparisons between in-vivo and ex-vivo measurements

There are main differences between investigations based on in-vivo measurements and post-mortem brain samples:

Resolution plays a major role. The difference in resolution between the imaging modalities used here is quite large and ranges from 0.5 mm isotropic resolution in in-vivo MRI measurements and 0.25 mm isotropic resolution in ex-vivo MRI measurements to 0.00258 mm = 2.58 μm in-plane resolution in our histological experiment. Thus, differences in sampled image values may arise from different partial volume effects.

Fixation of the ex-vivo sample may have an effect on the size of the cortical layers due to a small shrinking of the tissue during the fixation process (Mouritzen, 1978).

Transverse relaxation time is decreased after the fixation of a tissue sample. Thus, the dynamic range in the data is different. Mean T_1 values of GM derived from in-vivo MR data span a dynamic range of approximately 1500 ms. In MR data of a formalin-fixed brain sample, the mean T_1 values of GM span a range of approximately 350 ms.

Age difference between the in-vivo and ex-vivo measurements is very large. A T_1 map derived from older post-mortem brains may reveal slightly higher T_1 values. The change of the laminar myelin pattern across cortical depth may loose some significance in location of the bands of Baillarger (Lintl and Braak, 1983).

Limitations in histology

One should keep in mind that comparing profiles from different imaging modalities is difficult since each individual modality has its own limitations. Here, it is worth noting that the linear nature of myelinated axons and the planar dimensionality of myelin-stained cadaver brain sections make the problem of calculating 3D quantitative profiles representing myelin concentration directly from histology almost insuperable. The method cannot determine absolute values of myelin because even a highly standardised myelin staining process is not a quantitative method.

Summary and conclusion

The approach presented offers a fresh perspective for imaging and modelling the relationship between myelo- and cytoarchitecture, in the context of the increasing interest in advanced methods in brain segmentation and cortical architectural studies. Future work includes an extension of the modelling approach towards other cortical areas which are harder to parcellate, such as Broca's region. Theoretically, in turn, this approach can be used to estimate general patterns of cytoarchitecture from quantitative T_1 maps in locations where the cytoarchitecture is not well studied. Using proper cortical surface registration techniques (Tardif et al., 2013) may be beneficial in two ways: it could be helpful in studying group average myelin maps and lead to the construction of a digital probabilistic atlas. Thus, spatial distributions of myelin values in cortical grey matter can be studied. Increasing the sample size and the age range of the study will help to adjust the modelling, in particular considering that changes in cell and myelin morphology occur throughout human life span (Henderson et al., 1980; Terry et al., 1987).

Funding

This work was supported by the European Commission Research Executive Agency through the Marie-Curie-Programme (CIG08-GA-2010-276684-Highresbrain7t).

Acknowledgments

We would like to thank Prof. Rudolf Niewenhuys (Netherlands Institute for Neuroscience) for sharing his ideas and papers, and especially for the great discussions which have brought this work to its current stage. Special thanks go to Bernhard Hellwig for constructive discussions on his method and how to improve the given approach in order to apply it to MR brain imaging. We thank Daniel Rose for pushing the MP2RAGE sequence in post-mortem scanning at 7 T to 0.25 mm isotropic resolution and Markus Morawski (Paul Flechsig Institute for Brain Research, University Leipzig, Germany) for providing new ideas on staining protocols that have been tested and finalised by Katja Reimann. Last but not the least, we would like to thank Stefanie Quade (Otto von Guericke University, Magdeburg, Germany) for proofreading the manuscript and Christoph Leuze (Stanford University, USA) for sharing the paper on Hellwig's approach (Hellwig, 1993).

We would like to thank the Marie-Curie-Programme (276684-Highresbrain7t) for partially funding this work.

Appendix A. Supplementary data

Supplementary data to this article can be found online at http://dx.doi.org/10.1016/j.neuroimage.2015.04.023.

References

Annese, J., Pitiot, A., Dinov, I., Toga, A., 2004. A myelo-architectonic method for the structural classification of cortical areas. NeuroImage 21, 15–26.
Baillarger, J., 1840. Recherches sur la structure de la couche corticale des circonvolutions du cerveau. Mémoires de l'Académie Royale de Médecine vol. 8.
Bazin, P.L., Weiss, M., Dinse, J., Schäfer, A., Trampel, R., Turner, R., 2013. A computational framework for ultra-high resolution cortical segmentation at 7 Tesla. NeuroImage 93, 201–209.
Bock, N., Kocharyan, A., Liu, J., Silva, A., 2009. Visualizing the entire cortical myelination pattern in marmosets with magnetic resonance imaging. J. Neurosci. Methods 185, 15–22.
Bok, S., 1929. Der Einfluß der in den Furchen und Windungen auftretenden Krümmungen der Großhirnrinde auf die Rindenarchitektur. Z. Gesamte Neurol. Psychiatr. 121, 682–750.
Braitenberg, V., 1962. A note on myeloarchitectonics. J. Comp. Neurol. 118, 141–156.
Braitenberg, V., 1974. Thoughts on the cerebral cortex. J. Theor. Biol. 46, 421–447.

Bridge, H., Clare, S., 2006. High-resolution MRI: in vivo histology? Philos. Trans. R. Soc. Lond. B Biol. Sci. 361, 137–146.

Bridge, H., Clare, S., Jenkinson, M., Jezzard, P., Parker, A., Matthews, P., 2005. Independent anatomical and functional measures of the V1/V2 boundary in human visual cortex. J. Vis. 5, 93–102.

Brodmann, K., 1909. Vergleichende Lokalisationslehre der Großhirnrinde in ihren Prinzipien dargestellt auf Grund des Zellenbaues. JA Barth, Leipzig.

Callaghan, M., Freund, P., Draganski, B., Anderson, E., Cappelletti, M., Chowdhury, R., Diedrichsen, J., FitzGerald, T., Smittenaar, P., Helms, G., Lutti, A., Weiskopf, N., 2014. Widespread age-related differences in the human brain microstructure revealed by quantitative magnetic resonance imaging. Neurobiol. Aging 35, 1862–1872.

Clark, V., Courchesne, E., Grafe, M., 1992. In vivo myeloarchitectonic analysis of human striate and extrastriate cortex using magnetic resonance imaging. Cereb. Cortex 2, 417–424.

Cohen-Adad, J., Polimeni, J., Helmer, K., Benner, T., McNab, J., Wald, L., Rosen, B., Mainero, C., 2012. T_2^*-mapping and B_0 orientation-dependence at 7 T reveal cyto- and myeloarchitecture organization of the human cortex. NeuroImage 60, 1006–1014.

Colonnier, M., Sas, E., 1978. An anterograde degeneration study of the tangential spread of axons in cortical areas 17 and 18 of the squirrel monkey (*Saimiri sciureus*). J. Comp. Neurol. 179, 245–262.

Creutzfeldt, O., Garey, L., Kuroda, R., Wolff, J.R., 1977. The distribution of degenerating axons after small lesions in the intact and isolated visual cortex of the cat. Exp. Brain Res. 27, 419–440.

Deistung, A., Schäfer, A., Schweser, F., Biedermann, U., Turner, R., Reichenbach, J., 2013. Toward in vivo histology: a comparison of quantitative susceptibility mapping (QSM) with magnitude-, phase-, and R_2^*-imaging at ultra-high magnetic field strength. NeuroImage 65, 299–314.

Dick, F., Tierney, A., Lutti, A., Josephs, O., Sereno, M., Weiskopf, N., 2012. In vivo functional and myeloarchitectonic mapping of human primary auditory areas. J. Neurosci. 32, 16095–16105.

Dinse, J., Martin, P., Schäfer, A., Geyer, S., Turner, R., Bazin, P.L., 2013a. Quantifying differences between primary cortical areas in humans based on laminar profiles in in-vivo MRI data. In: Meinzer, H.P., Deserno, T., Handels, H., Tolxdorff, T. (Eds.), Bildverarbeitung für die Medizin 2013. Springer, pp. 39–44.

Dinse, J., Waehnert, M., Tardif, C., Schäfer, A., Geyer, S., Turner, R., Bazin, P.L., 2013b. A histology-based model of quantitative T1 contrast for in-vivo cortical parcellation of high-resolution 7 Tesla brain MR images. Medical Image Computing and Computer-Assisted Intervention—MICCAI 2013. Springer, pp. 51–58.

Eickhoff, S., Stephan, K., Mohlberg, H., Grefkes, C., Fink, G., Amunts, K., Zilles, K., 2005a. A new SPM toolbox for combining probabilistic cytoarchitectonic maps and functional imaging data. NeuroImage 25, 1325–1335.

Eickhoff, S., Walters, N., Schleicher, A., Kril, J., Egan, G., Zilles, K., Watson, J., Amunts, K., 2005b. High-resolution MRI reflects myeloarchitecture and cytoarchitecture of human cerebral cortex. Hum. Brain Mapp. 24, 206–215.

Fischl, B., Rajendran, N., Busa, E., Augustinack, J., Hinds, O., Yeo, B., Mohlberg, H., Amunts, K., Zilles, K., 2008. Cortical folding patterns and predicting cytoarchitecture. Cereb. Cortex 18, 1973–1980.

Fisken, R.A., Garey, L., Powell, T., 1975. The intrinsic, association and commissural connections of area 17 of the visual cortex. Philos. Trans. R. Soc. Lond. Ser. B Biol. Sci. 272, 487–536.

Gatter, K., Sloper, J., Powell, T., 1978. The intrinsic connections of the cortex of area 4 of the monkey. Brain 101, 513–541.

Gennari, F., 1782. De peculiari structura cerebri, nonnullisque ejus morbis. Ex Regio Typographeo, Parma.

Geyer, S., Schleicher, A., Zilles, K., 1999. Areas 3a, 3b, and 1 of human primary somatosensory cortex: 1. Microstructural organization and interindividual variability. NeuroImage 10, 63–83.

Geyer, S., Weiss, M., Reimann, K., Lohmann, G., Turner, R., 2011. Microstructural parcellation of the human cerebral cortex—from Brodmann's post-mortem map to in vivo mapping with high-field magnetic resonance imaging. Front. Hum. Neurosci. 5.

Glasser, M., Van Essen, D., 2011. Mapping human cortical areas in vivo based on myelin content as revealed by T1- and T2-weighted MRI. J. Neurosci. 31, 11597–11616.

Grefkes, C., Geyer, S., Schormann, T., Roland, P., Zilles, K., 2001. Human somatosensory area 2: observer-independent cytoarchitectonic mapping, interindividual variability, and population map. NeuroImage 14, 617–631.

Hallgren, B., Sourander, P., 1958. The effect of age on the non-haemin iron in the human brain. J. Neurochem. 3, 41–51.

Han, X., Xu, C., Prince, J., 2003. A topology preserving level set method for geometric deformable models. IEEE Trans. Pattern. Anal. Mach. Intell. 25, 755–768.

Han, X., Pham, D., Tosun, D., Rettmann, M., Xu, C., Prince, J., 2004. CRUISE: cortical reconstruction using implicit surface evolution. NeuroImage 23, 997–1012.

Hellwig, B., 1993. How the myelin picture of the human cerebral cortex can be computed from cytoarchitectural data. A bridge between von Economo and Vogt. J. Hirnforsch. 34, 387–402.

Henderson, G., Tomlinson, B., Gibson, P., 1980. Cell counts in human cerebral cortex in normal adults throughout life using an image analysing computer. J. Neurol. Sci. 46, 113–136.

Hopf, A., 1955. Über die Verteilung myeloarchitektonischer Merkmale in der isokortikalen Schläfenlappenrinde beim Menschen. J. Hirnforsch. 2, 36–54.

Hopf, A., 1956. Über die Verteilung myeloarchitektonischer Merkmale in der Stirnhirnrinde beim Menschen. J. Hirnforsch. 2, 311–333.

Hopf, A., 1967. Registration of the myeloarchitecture of the human frontal lobe with an extinction method. J. Hirnforsch. 10, 259–269.

Hopf, A., 1968. Photometric studies on the myeloarchitecture of the human temporal lobe. J. Hirnforsch. 10, 285–297.

Hopf, A., 1969. Photometric studies on the myeloarchitecture of the human parietal lobe. I. Parietal region. J. Hirnforsch. 11, 253–265.

Hopf, A., 1970. Photometric studies on the myeloarchitecture of the human parietal lobe. II. Postcentral region. J. Hirnforsch. 12, 135–141.

Hopf, A., Vitzthum, H.G., 1957. Über die Verteilung myeloarchitektonischer Merkmale in der Scheitellappenrinde beim Menschen. J. Hirnforsch. 3, 79–104.

Hurley, A., Al-Radaideh, A., Bai, L., Aickelin, U., Coxon, R., Glover, P., Gowland, P., 2010. Tailored RF pulse for magnetization inversion at ultrahigh field. Magn. Reson. Med. 63, 51–58.

Jäger, C., Lendvai, D., Seeger, G., Brückner, G., Matthews, R., Arendt, T., Alpar, A., Morawski, M., 2013. Perineuronal and perisynaptic extracellular matrix in the human spinal cord. Neuroscience 238, 168–184.

Lashkari, D., Sridharan, R., Vul, E., Hsieh, P.J., Kanwisher, N., Golland, P., 2010. Nonparametric hierarchical Bayesian model for functional brain parcellation. 2010 IEEE Computer Vision and Pattern Recognition Workshops (CVPRW), pp. 15–22.

Le Gros Clark, W., Sunderland, S., 1939. Structural changes in the isolated visual cortex. J. Anat. 73, 563–574.

Lintl, P., Braak, H., 1983. Loss of intracortical myelinated fibers: a distinctive age-related alteration in the human striate area. Acta Neuropathol. 61, 178–182.

Lucas, B., Bogovic, J., Carass, A., Bazin, P.L., Prince, J., Pham, D., Landman, B., 2010. The Java Image Science Toolkit (JIST) for rapid prototyping and publishing of neuroimaging software. Neuroinformatics 8, 5–17.

Lutti, A., Dick, F., Sereno, M., Weiskopf, N., 2014. Using high-resolution quantitative mapping of R_1 as an index of cortical myelination. NeuroImage 93, 176–188.

Marques, J., Kober, T., Krueger, G., van der Zwaag, W., Van de Moortele, P., Gruetter, R., 2010. MP2RAGE, a self bias-field corrected sequence for improved segmentation and T_1-mapping at high field. NeuroImage 49, 1271–1281.

Mouritzen, D., 1978. Shrinkage of the brain during histological procedures with fixation in formaldehyde solutions of different concentrations. J. Hirnforsch. 20, 115–119.

Nieuwenhuys, R., 2013. The myeloarchitectonic studies on the human cerebral cortex of the Vogt–Vogt School, and their significance for the interpretation of functional neuroimaging data. Brain Struct. Funct. 218, 303–352.

Nieuwenhuys, R., Broere, C., Cerliani, L., 2014. A new myeloarchitectonic map of the human neocortex based on data from the Vogt–Vogt School. Brain Struct. Funct. 1–23.

Paldino, A., Harth, E., 1977. Some quantitative results on Golgi impregnated axons in rat visual cortex using a computer assisted video digitizer. J. Comp. Neurol. 176, 247–261.

Peters, A., 2002. The effects of normal aging on myelin and nerve fibers: a review. J. Neurocytol. 31, 581–593.

Robinson, E., Jbabdi, S., Andersson, J., Smith, S., Glasser, M., Van Essen, D., Burgess, G., Harms, M., Barch, D., Jenkinson, M., 2013. Multimodal surface matching: fast and generalisable cortical registration using discrete optimisation. In: Gee, J., Joshi, S., Pohl, K., Wells, W., Zöllei, L. (Eds.), Information Processing in Medical Imaging. Springer, pp. 475–486.

Rooney, W., Johnson, G., Li, X., Cohen, E., Kim, S., Ugurbil, K., Springer, C., 2007. Magnetic field and tissue dependencies of human brain longitudinal $1H_2O$ relaxation in vivo. Magn. Reson. Med. 57, 308–318.

Ryali, S., Chen, T., Supekar, K., Menon, V., 2012. A parcellation scheme based on von Mises–Fisher distributions and Markov random fields for segmenting brain regions using resting-state fMRI. NeuroImage 65, 83–96.

Sabuncu, M., Yeo, B., Van Leemput, K., Fischl, B., Golland, P., 2009. Nonparametric mixture models for supervised image parcellation. In: Yang, G., Hawkes, D., Rueckert, D., Noble, A., Taylor, C. (Eds.), Medical Image Computing and Computer-Assisted Intervention — MICCAI 2009. NIH Public Access, Springer, pp. 301–313.

Sanides, F., 1962. Die Architektonik des menschlichen Stirnhirns: zugleich eine Darstellung der Prinzipien seiner Gestaltung als Spiegel der stammesgeschichtlichen Differenzierung der Grosshirnrinde. Springer.

Schleicher, A., Palomero-Gallagher, N., Morosan, P., Eickhoff, S., Kowalski, T., Vos, K., Amunts, K., Zilles, K., 2005. Quantitative architectural analysis: a new approach to cortical mapping. Anat. Embryol. 210, 373–386.

Schulz, J., Siegert, T., Reimer, E., Labadie, C., Maclaren, J., Herbst, M., Zaitsev, M., Turner, R., 2012. An embedded optical tracking system for motion-corrected magnetic resonance imaging at 7 T. MAGMA 25, 443–453.

Sereno, M., Lutti, A., Weiskopf, N., Dick, F., 2012. Mapping the human cortical surface by combining quantitative T_1 with retinotopy. Cereb. Cortex 23, 2261–2268.

Sethian, J., 1999. Level Set Methods and Fast Marching Methods: Evolving Interfaces in Computational Geometry, Fluid Mechanics, Computer Vision, and Materials Science. Cambridge University Press, p. 3.

Smith, G., 1907. A new topographical survey of the human cerebral cortex, being an account of the distribution of the anatomically distinct cortical areas and their relationship to the cerebral sulci. J. Anat. Physiol. 41, 237–254.

Stüber, C., Morawski, M., Schäfer, A., Labadie, C., Wähnert, M., Leuze, C., Streicher, M., Barapatre, N., Reimann, K., Geyer, S., Spemann, D., Turner, R., 2014. Myelin and iron concentration in the human brain: a quantitative study of MRI contrast. NeuroImage 93 (Part 1), 95–106.

Tardif, C., Dinse, J., Schäfer, A., Turner, R., Bazin, P.L., 2013. Multi-modal surface-based alignment of cortical areas using intra-cortical T1 contrast. In: Shen, L., Liu, T., Yap, P.T., Huang, H., Shen, D., Westin, C.F. (Eds.), Multimodal Brain Image Analysis vol. 8159. Springer, pp. 222–232.

Terry, R., DeTeresa, R., Hansen, L., 1987. Neocortical cell counts in normal human adult aging. Ann. Neurol. 21, 530–539.

Vicq d'Azyr, F., 1786. Traité d'anatomie et de physiologie: Planches Anatomiques. F. A. Didot, Paris.

Vogt, O., 1910. Die myeloarchitektonische Felderung des menschlichen Stirnhirns. J. Psychol. Neurol. 15, 221–232.

Vogt, O., 1923. Furchenbildung und architektonische Rindenfelderung. J. Psychol. Neurol. 29, 438–439.

Vogt, C., Vogt, O., 1919a. Allgemeinere Ergebnisse unserer Hirnforschung. Erste Mitteilung. Ziele und Wege unserer Hirnforschung. J. Psychol. Neurol. 25, 281–291.
Vogt, C., Vogt, O., 1919b. Allgemeinere Ergebnisse unserer Hirnforschung. Zweite Mitteilung. Das Wesen der topischen architektonischen Differenzen des Cortex cerebri. J. Psychol. Neurol. 25, 292–360.
von Economo, C., Koskinas, G., 1925. Die Cytoarchitektonik der Hirnrinde des Erwachsenen Menschen. Textband und Atlas, Wien und Berlin.
Waehnert, M., Dinse, J., Tardif, C., Schäfer, A., Geyer, S., Bazin, P.L., Turner, R., 2013a. How much resolution is needed for in-vivo analysis of cortical myeloarchitecture? Proceedings of ISMRM 2013, Abstract 270
Waehnert, M., Dinse, J., Weiss, M., Streicher, M., Waehnert, P., Geyer, S., Turner, R., Bazin, P.L., 2013b. Anatomically motivated modeling of cortical laminae. NeuroImage 93, 210–220.
Walters, N., Egan, G., Kril, J., Kean, M., Waley, P., Jenkinson, M., Watson, J., 2003. In vivo identification of human cortical areas using high-resolution MRI: an approach to cerebral structure–function correlation. Proc. Natl. Acad. Sci. 100, 2981–2986.
Walters, N., Eickhoff, S., Schleicher, A., Zilles, K., Amunts, K., Egan, G., Watson, J., 2007. Observer-independent analysis of high-resolution MR images of the human cerebral cortex: in vivo delineation of cortical areas. Hum. Brain Mapp. 28, 1–8.